Chapter 2
Phosphors for Field Emission Display: Recent Advances in Synthesis, Improvement, and Luminescence Properties

Guogang Li and Jun Lin

Abstract Field emission displays (FEDs) have been considered as one of the most promising next-generation flat panel display (FPD) technologies due to its excellent display performances and low energy consumption. Phosphors are irreplaceable components for FEDs. The exploration of highly efficient low-voltage FED phosphors is the focus of enhancing energy efficiency and realizing high-quality display. This chapter summarizes the recent progress in chemical synthesis and improvement of rare earth and transition metal ion-activated inorganic FEDs phosphors with powder and thin film forms. Discussion is focused on the modification of morphology, size, surface, composition, conductivity of phosphors, and corresponding effects on their cathodoluminescent properties. Special emphases are given to the selection of host and luminescent centers, the adjustment of emission colors through doping concentration optimization, energy transfer, mono- or codoping activator ions, the improvement of chromaticity, color stability and color gamut as well as the saturation behavior and the degradation behavior of phosphors under the excitation of low-voltage electron beam. The authors also speak about the research prospects and future directions of FED phosphors and give some recommendations to facilitate the further exploration of new and highly efficient low-voltage FED phosphors.

G. Li
Faculty of Materials Science and Chemistry, China University of Geosciences, Wuhan 430074, People's Republic of China
e-mail: ggli8312@gmail.com

J. Lin (✉)
State Key Laboratory of Rare Earth Resource Utilization, Changchun Institute of Applied Chemistry, Chinese Academy of Sciences, Changchun 130022, People's Republic of China
e-mail: jlin@ciac.ac.cn

R.S. Liu (ed.), *Phosphors, Up Conversion Nano Particles, Quantum Dots and Their Applications*, DOI 10.1007/978-981-10-1590-8_2

2.1 Introduction

So far, quite a few technologies have been developed for flat panel displays (FPDs), including plasma display panels (PDPs), electroluminescence (EL) devices, field emission displays (FEDs), and liquid crystal displays (LCDs). Of these display technologies, in recent years, FEDs have been considered as one of the most promising technologies for next-generation FPDs due to their potential advantages in aspects of display quality (brightness, contrast ratio, angle of viewing, response time), power consumption, stability, lifetime, etc. [1]. Currently, developing display panel technologies with enhanced energy efficiency and improved display quality is strongly stimulated, because people have more and more requirements for image quality. For FEDs, its basis is an array of field emitter tip cathodes aligned opposite to the phosphor anode, as shown in Fig. 2.1. Therefore, the development of FEDs mainly depends on the following aspects: electron-emitting microcathode arrays, the packaging of FED devices, and luminescent materials. Especially, the luminescent materials (or phosphors) are indispensable components of FED devices, whose luminescent efficiencies and properties not only determine the quality of images but also affect the energy efficiency of display devices [2–4]. Therefore, the selection of phosphors is critical for FEDs. In the past decade, the exploration and development of highly efficient low-voltage FED phosphors and improvement of existing FED phosphors have been becoming the focus of developing FED devices [5–10].

Basically, the operation principle of FEDs is similar to that of conventional cathode ray tubes (CRTs) in which the images originate from the excitation of electrons on phosphors (Fig. 2.1). However, requirements for phosphors applied in FEDs are greatly different from those used in CRTs due to the lower accelerating

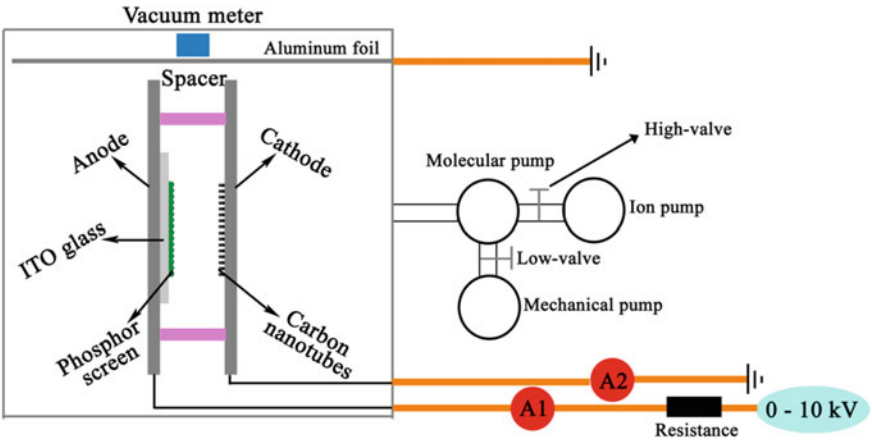

Fig. 2.1 A schematic model of analogue FEDs device. Adapted from Ref. [51] by permission of Optical Society of America

voltages and the higher current densities. One hand, FED phosphors should decrease or avoid the release of gasses in the FED devices [11]. On the other hand, it should posses excellent cathodoluminescent properties such as high emission intensity, high luminous efficiency, high saturation current density, high color purity, and good stability and durability under low accelerating voltages (≤7 kV) and high current density (≥100 μA/cm^2) [12, 13]. Therefore, the selection of suitable hosts and luminescent centers is very important for synthesis of FED phosphors [14]. As activator ions, rare earth (RE) ions have been playing an important role in modern lighting and display fields due to the abundant emission colors in the whole visible light range owing to their $4f \rightarrow 4f$ or $5d \rightarrow 4f$ transitions [15]. In addition, transition metal ion (Mn^{2+}), Bi^{3+} ion, and some groups (e.g., WO_4^{2-}, MoO_4^{2-}, GeO_4^{4-}, SnO_6^{2-}, TiO_6^{2-}, NbO_4^{2-}) are also efficient luminescent centers [16–20]. For host materials, so far many efficient sulfide-based phosphors such as $Y_2O_2S:Eu^{3+}$, $Gd_2O_2S:Tb^{3+}$, $SrGa_2S_4:Eu^{3+}/Ce^{3+}$, (Zn/Cd)S:Cu,Al, and ZnS:Ag,Cl have been explored as efficient low-voltage FED phosphors [21, 22]. Unfortunately, sulfide phosphors are easily decomposed and emit sulfide gases under electron bombardment due to dissociation of the cation–sulfur bonds, subsequently damage emission tips, shorten the device lifetime, and simultaneously contaminate environment. In avoidance of the above defects, oxide-based phosphors including rare earth and transition metal ion-doped garnets, oxides, silicates, phosphates, vanadates, and perovskites [23–29] have gained increasing concerns due to their better thermal stability, chemical stability, and environmental friendliness compared with sulfides. However, most of these phosphors are insulators, and negative loading is easy to accumulate on the grain surface in phosphor layer, which decreases cathodoluminescent efficiency. That is why the electrical conductivity of FED phosphors should be high enough to avoid charge accumulation [12]. In recent years, many semiconductor-based materials such as ZnO, Ga_2O_3, $(Gd,Lu)_3Ga_5O_{12}$, $Zn(Ga,In)_2O_4$, $(Ca,Sr)In_2O_4$, $Zn_3Ta_2O_8$, Zn_2GeO_4, $GaGe_2O_5$, Mg_2SnO_4, and $ZnGeN_2$ are explored as low-voltage FED phosphors through efficiently doping of RE^{3+}, Mn^{2+}, and Bi^{3+} ions [7, 23, 26, 28, 30–38]. Besides, the current low-voltage FED phosphors also suffer rough surfaces, irregular shape and size distribution, poor adherence to substrates, poor preparing of phosphor screens (thin films) from phosphor powders. Therefore, more efforts should explore excellent approaches for the fabrication of a variety of inorganic luminescence materials to improve their performance in applications. Finally, the color saturation and color index also need be further improved to enhance display quality. All these considerations and the ever-growing demand for highly efficiently low-voltage FED phosphors prompt researchers to reach a cognitive that more attention should be paid to improve existing phosphors and develop newly efficient low-voltage FED phosphors. This chapter mainly summarizes the recent progress in chemical synthesis and improvement of existing and new phosphors including RE^{3+} ions and transition metal ion-activated inorganic oxide-based luminescence materials, semiconductor-based luminescence materials, and self-activated luminescent materials. The authors discuss the modifications and optimizations in morphology,

size, composition, conductivity of phosphors, and their cathodoluminescent properties. Some emphases are also focused on the studies of selection of hosts and luminescent centers, enhancement of efficiency through energy transfer, adjustment and design of emission colors, improvement of color index, and color gamut as well as color stability and degradation behavior of phosphors.

2.2 Improvement of Current FED Phosphor Powders

2.2.1 Modification of Morphology, Surface, and Size of Phosphor Particles

It is well known that the most common form of phosphors is powders, which are conventionally prepared by the solid reaction process. Unfortunately, this process might result in a damage of luminescent performance of phosphors due to irregular shapes, wide size distribution, and serious aggregation of the final phosphor products [39]. Because the morphology, size, composition, surface, and crystallization have great effects on the cathodoluminescent properties of phosphors, many efforts have been made to explore suitable methods to control these factors for improving their cathodoluminescent performance, which has technological and fundamental scientific importance [40]. Among them, the soft-chemical methods (such as sol–gel, hydrothermal, spray pyrolysis, electrospinning, homogenous precipitation, high boiling solvent, combustion, and microwave) are intensively pursed as effective and convenient approaches to prepare various inorganic FED phosphors with controllable shape, size, surface form, composition, and luminescent properties [32, 41–45]. In general, soft-chemistry synthesis can produce future generation phosphors with better morphology and surface forms (more regular shape, spherical in some cases), and narrower size dispersions at moderate temperatures (<1000 °C). These factors can decrease the light scattering and non-radiative transitions of phosphors, which is conducive to enhance the cathodoluminescent performance.

On the other hand, for FED phosphor powders, the particle size is critical to loading on screens, which further influences their luminescent performance [12]. It is known that the cathodoluminescent emission intensities and brightness of FED phosphors increase with increasing the accelerating voltage and the filament current of anodes, which is attributed to the deeper penetration of the electrons into the phosphor body and the larger electron beam current density. The electron penetration depth can be estimated using the empirical formula:

$$L[\text{Å}] = 250\left(\frac{A}{\rho}\right)\left(\frac{E}{\sqrt{Z}}\right)^{n}, \quad n = \frac{1.2}{1 - 0.29\lg Z}$$

where $n = 1.2/(1 - 0.29\ \lg Z)$, and A is the atomic or molecular weight of the material, ρ is the bulk density, Z is the atomic number or the number of electrons per molecule in the compounds, and E is the accelerating voltage (kV) [41]. The deeper the electron penetration depth, the more plasma will be produced, which results in the CL intensity increases. However, according to the above empirical formula, the electron penetration depth into phosphors are general tens of nanometers in FEDs devices due to the low excition voltage (1–7 kV), which makes activator ions in the inner of phosphor particles with big size (microsize) cannot be efficiently excited. So, reasonable particle size is important for improving their cathodoluminescent efficiencies. Nanoparticle phosphors might be more appropriate for low-voltage FED application in terms of the following aspects [12, 46]: (1) The resolution is inversely proportional to the particle size of the luminescent materials; (2) the use of such materials can optimize the packaging of grains, avoid cutting of the picture spot and decrease scattering of light-emitting; (3) phosphor powders with small grain size allow a fabrication of thin light-emitting film, which could extend the display operating time and fundamentally decreased the total resistance of phosphor layer. Therefore, some researchers try hard to obtain low-voltage FED phosphors in nanosize via various soft-chemical synthesis processes for improving their luminescence efficiency. Some possible routes to achieve the above improvements are presented in the following section.

Sol–gel process. The sol–gel technique is one of the most well-known soft-chemistry processes, which can be generally divided into three types judging by different use of precursors [47]: (a) sol–gel process under hydrolysis and condensation of molecular precursors; (b) gelation process under concentration of aqueous solutions into metal chelates, namely "chelate" route; (c) polymerization and complex process (called Pechini-type sol–gel process, and abbreviate as PSG). Among the three types, PSG process is frequently employed in the preparation of multicomponent metal oxide materials. This process commonly uses metal salts as precursors, citric acid (CA) as a chelating ligand of metal ions, and polyhydroxy alcohol such as ethylene glycol (EG) or poly(ethylene glycol) (PEG) as a cross-linking agent to form a polymeric resin on the molecular level, which can ensure compositional homogeneity and enhance dispersion of particles. After a heat treatment at moderate temperature (500–1000 °C) followed by PSG process, the organic additives can be removed and a pure phase of multiple-component metal oxide is obtained. The final materials (including luminescent materials) can be made into powder and thin film forms and others. By PSG process, the physical properties of materials can be improved with respect to the other routes such as solid-state reaction process and amorphous citrate process [47]. Recently, Lin's groups have derived multiformed FED phosphors from the PSG process, including nanocrystalline luminescent materials, monodisperse and spherical core–shell-structured phosphors, one-dimensional (1D) nanostructures (combined with the electrospinning process), thin film phosphors (via dip-coating), and their patterning (combined with the soft-lithography process). The basic principle is shown in Fig. 2.2. The purpose was to gain fine control of the material morphology, surface, and size, and to find novel FEDs phosphors and optimize their

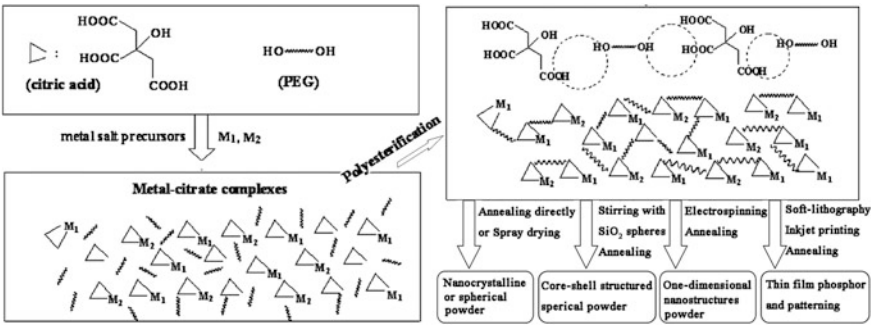

Fig. 2.2 Basic principle of Pechini-type sol–gel (PSG) process and multiform optical materials derived from it. Adapted from Ref. [47] by permission of American Chemical Society

cathodoluminescent performance. Typically, a series of oxide-based nanocrystalline phosphors from tens of nanometers to several hundred of nanometers have been prepared through the PSG process for FEDs, including $LaOCl/LaGaO_3/LaAlO_3$:RE^{3+} [41, 48, 49], $Lu_3Ga_5O_{12}$:RE^{3+} [50], (Ca,Sr)In_2O_4:RE^{3+} (RE = Pr, Sm, Eu, Tb, Dy, Ho, Er, Tm) [26, 36], $NaCaPO_4$:Mn^{2+} [51], $KNaCa_2(PO_4)_2$:A (A = Ce^{3+}, Eu^{2+}, Tb^{3+}, Mn^{2+}, Sm^{3+}) [52], K(Sr,Ca)$Gd(PO_4)_2$:RE^{3+}/Mn^{2+} (RE = Ce, Tb, Dy, Eu, Tm) [53], $Ca_2Ba_3(PO_4)_3Cl$:A [54], $Ca_8Gd_2(PO_4)_6O_2$:A (A = Eu^{2+}, Ce^{3+}, Dy^{3+}, Tb^{3+}, Mn^{2+}) [55]. It is found that the nanocrystalline phosphor layer could be much thinner compared to that consists of microsize phosphor grains, which can influence both total resistivity of the phosphor layer and amount of residual gasses bounded between the grains [12]. Then, it further influences the efficiency of the light source, longtime stability of the intensity of emitted light, and device lifetime. Psuja et al. [12] investigated the effect of grain sizes on emission yield of RE-doped nanophosphors in cases of Eu^{3+}:Y_2O_3, Tb^{3+}:Y_2O_3, Tb^{3+}:$Y_3Al_5O_{12}$ (Tb:YAG), Ce^{3+}:YAG, and Tb^{3+}:YAG/Eu^{3+}:YAG. It was found that the light-emitting efficiencies increase with grain size in the nanorange by a comparison of cathodoluminescent intensities of phosphor layer and powders, and Eu:Y_2O_3 nanopowder was more efficient than commercially available microsize phosphor grains. Xu et al. [33] demonstrated that these as-prepared nanocrystalline phosphors ($Lu_3Ga_5O_{12}$:Tb^{3+}) by PSG process can form a more compact phosphor screen, which exhibits an improved luminescent efficiency and stability under the bombardment of electron beam. Wakefield et al. [56] also confirmed that the nanocrystalline oxide-based phosphors (Y_2O_3:Eu and Zn_2SiO_4:Mn) had better luminescence efficiency than that of commercial FED phosphors, which show promising properties for use in low-voltage FEDs.

Homogenous precipitation process. Homogenous precipitation process is a simple, effective solution-based method for a large-scale fabrication of novel inorganic nano-/microstructured materials under template-free conditions. It is usually used to synthesize hydroxide materials under different precipitants using metal salts as precursors [42]. After an annealing process at moderate temperature,

the obtained hydroxides can be transformed to oxide materials with maintaining morphology. Over the past several years, monodisperse nano-/microstructures with controllable morphologies and sizes, which exhibit size-dependent luminescent properties, have been synthesized by the homogenous precipitation and investigated. For example, Li et al. have reported the simple synthesis of monodisperse β-Ga_2O_3:Dy^{3+} [32], La_2O_3/$La_2O_2CO_3$:RE^{3+} (RE = Eu, Tb, Yb, Ho, Er, Tm) [42], etc., with defined morphologies and narrow size dispersion (Fig. 2.3a, b) by optimizing the external experimental parameters. They demonstrated that the cathodoluminescent properties of phosphors can be improved by improving the morphologies and sizes of phosphors particles. As shown in Fig. 2.3c, the relative CL emission intensities of β-Ga_2O_3:Dy^{3+} phosphors are different with different morphologies/sizes, which are attributed to the difference in surface defects. The more defects on phosphor particles surface, the lower luminescent efficiency are obtained due to the increase in non-radiative transitions. The similar situation appears in the as-prepared La_2O_3/$La_2O_2CO_3$:RE^{3+} (RE = Eu, Tb) phosphor particles with different shapes and sizes (Fig. 2.3d). Jung et al. [57] also improved the

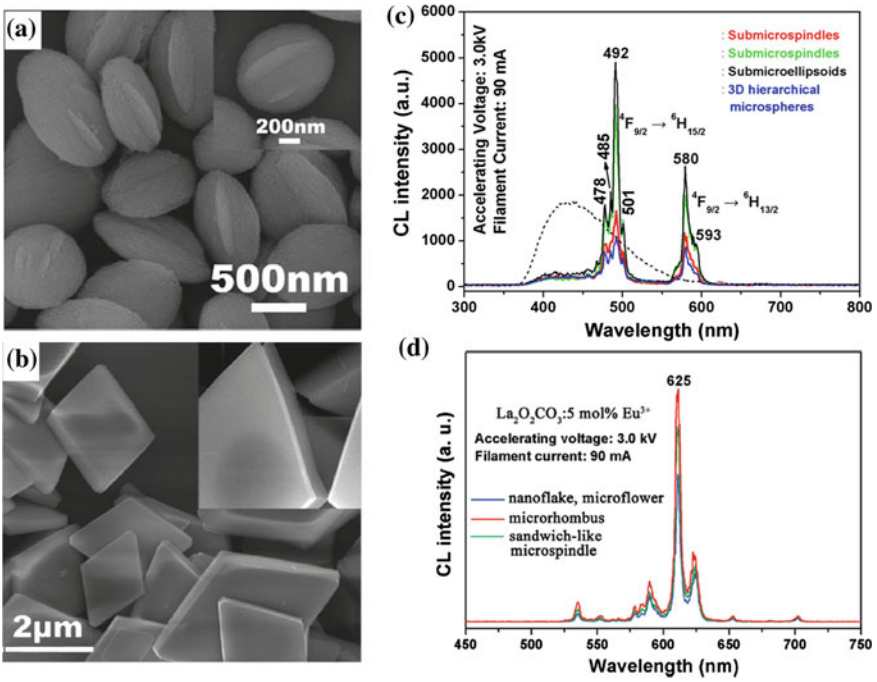

Fig. 2.3 SEM image of **a** GaOOH:Dy^{3+} and **b** $LaCO_3OH$:Eu^{3+} prepared at pH = 7. Following a heat treatment, the above samples are, respectively, transformed to β-Ga_2O_3:Dy^{3+} and $La_2O_2CO_3$/La_2O_3:Eu^{3+} phosphors without changing morphologies. **c**, **d** show the comparison of CL and photoluminescent (PL) emission intensity of β-Ga_2O_3:Dy^{3+} and $La_2O_2CO_3$:Eu^{3+} at different morphologies and sizes. **a**, **c** Adapted from Ref. [32] by permission of American Chemical Society. **b**, **d** Adapted from Ref. [42] by permission of American Chemical Society

luminance of Zn_2SiO_4:Mn phosphors by homogenous precipitation process. The as-prepared Zn_2SiO_4:Mn phosphor particles present uniform spherical shape and have an enhanced emission intensity than commercial Zn_2SiO_4:Mn bulk phosphors. In addition, spherical sub-micrometer Y_2O_3:Eu^{3+} and cubic $(Y, Gd)_2O_3$:Eu^{3+} phosphor particles have been synthesized through a novel homogeneous precipitation method by Silver et al. [58]. These cubic-Y_2O_3:Eu^{3+} spherical phosphor particles (ca. 300 nm) will be ideal for FED devices as they can densely close-pack on screens and they display high luminous efficiency under low-voltage electron beam excitation. The above examples demonstrate through the modification of morphology, size, and surface, one can reduce surface defects and thus enhance the luminescent efficiencies of phosphors.

Hydro/solvothermal process. As a typical solution-based approach, hydro-/solvothermal process generally employs water or organic solvents under certain temperatures and pressures for synthesis of variously inorganic nano- and/or micro-crystals due to some acceptable advantages including relatively green synthesis, easily controllable reaction conditions, low reaction temperature (in general <250 °C) and cost, high yield, specially, easily controlled size, structure and shapes of the products. Shang et al. [38] developed a water-based hydrothermal system to prepare Zn_2GeO_4:Mn^{2+} phosphors with irregular submicrorods shape. Annealing at different temperatures can remove H_2O and organic components on surface, and then obtain Zn_2GeO_4:Mn^{2+} submicrorods phosphors, as shown in Fig. 2.4a–d. It is obviously seen that Zn_2GeO_4:Mn^{2+} submicrorod phosphor has smooth surface, regular shape, and narrow size distribution than bulk material prepared by solid-state reaction method. Under the same excitation conditions, Zn_2GeO_4:Mn^{2+} submicrorod phosphor has a higher CL emission intensity than that of bulk materials (Fig. 2.4e). Because of the optimal shape, size, and surface of particles, the cathodoluminescent efficiency of Zn_2GeO_4:Mn^{2+} phosphor was enhanced. During the process of hydro-/solvothermal reaction, selecting an

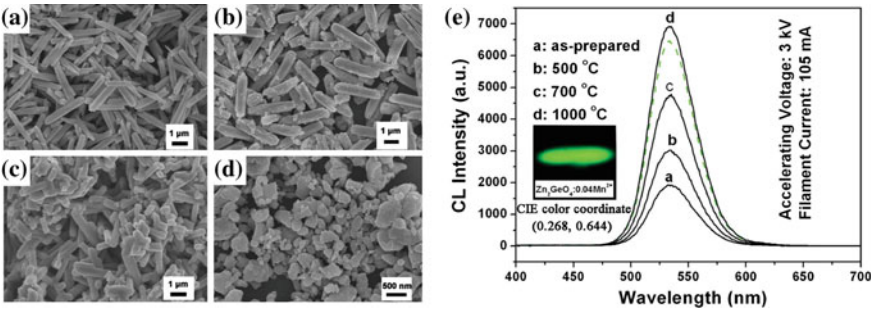

Fig. 2.4 **a–d** SEM images and **e** CL spectra of Zn_2GeO_4:Mn^{2+} submicrorods with different post-calcination temperatures: 500, 700, 1000 °C and Zn_2GeO_4:Mn^{2+} bulk material (solid-state reaction process), respectively. The *insets* in **e** show the luminescent photographs of Zn_2GeO_4:Mn^{2+} with highly pure *green light* emission. Adapted from Ref. [38] by permission of Royal Society of Chemistry

appropriate organic additive with functional groups is one of the promising and popular strategies to control shape and size. The organic additive generally acts as complex agent or structure-directing agent. Through using oleic acid in reaction system, Shang et al. [59] successfully prepared well-separated LaOF:RE^{3+} (RE = Eu^{3+}, Ho^{3+}, Tm^{3+}, Dy^{3+}, Sm^{3+}, Tb^{3+}) nanoparticles with sizes of about 30–50 nm. Due to the excellent dispersion and crystallinity, these as-prepared LaOF:RE^{3+} phosphor nanoparticles can also be compactly coated on screen to improve the intensity of emitted light, and device lifetime. Doping RE^{3+} ions into LaOF host, emission colors from blue to red with high color purity (4*f*–4*f* transition, Eu^{3+}, red; Ho^{3+}, green; Tm^{3+}, blue; Dy^{3+}, yellow; Sm^{3+}, orange) were obtained, which can be considered as potential full-color FED phosphors. In addition, the morphology and size of products can also be well controlled and modified by a combination of water and organic solvents in hydrothermal process. During these fabrication processes, organic solvents act as the "shape modifier" to either promote or inhibit crystal growth through modifying crystal growth dynamically and thus can adjust and control the morphology and size of the products. By the use of the above synthesis method, a series of FED phosphors such as β-Ga_2O_3:Dy^{3+} [32], Gd_2O_3:Eu^{3+} [60], Lu_2O_3:RE^{3+} (RE = Eu, Tb, Dy, Pr, Sm, Er, Ho, Tm) [61] with regular prism, rod, sphere shapes in nano- to microscale were synthesized, which not only improve the cathodoluminescent performances of phosphors but also meet some requirements in micromation of FED devices.

Electrospinning process. Because of some specific and fascinating luminescence properties, for example, various emission lifetimes and increased luminescence efficiencies, there is growing interest on exploring new luminescent materials on one-dimensional (1D) nanostructures [19, 62–65]. These one-dimensional luminescence nanomaterials possess diverse potential applications in nanoscale electronics, photonics, display and advanced bioanalysis [19]. The electrospinning technique is an effective and simple method for preparing one-dimensional (1D) nanomaterials. It is a process that uses the strong electrostatic force from a high static voltage act on a polymer solution placed in a container with a millimeter diameter nozzle. Under applied electrical force, the polymer solution is ejected from the nozzle. After the solvents are evaporated during the course of jet spraying, the fibers are collected on a grounded collector. The electrospinning setup and formation process of 1D luminescent nano-/microstructures is shown in Fig. 2.5a. 1D nanomaterials synthesized by this method followed an annealing process usually have exceptional long length, uniform diameter, and diverse composition. Through the electrospinning process, a variety of RE^{3+} ions doped 1D fiber-, tube- and belt-like cathodoluminescence materials including LaOCl [40], $CaTiO_3$ [63], $LaPO_4$ [64], YVO_4 [65], Y_2SiO_5 [66] etc. have been derived and/or optimized, especially morphology-/size-dependent luminescence were investigated and color tuning by doping different kinds of RE^{3+} ions, changing RE^{3+} ions concentrations, codoping and/or energy transfer were designed. For example, the as-prepared LaOCl:Eu^{3+} 1D nanofiber, nanotube, and microbelt phosphors are all composed of nanoparticles with perfect crystallinity, as shown in Fig. 2.5a. The comparison of CL spectra of 1D LaOCl:Eu^{3+} nanomaterials with three different

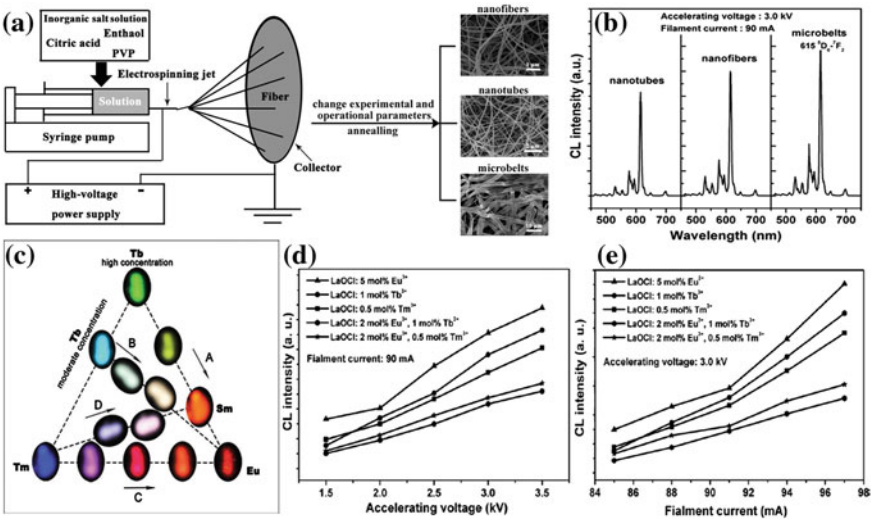

Fig. 2.5 **a** Scheme of the electrospinning setup and the formation process of 1D luminescence nano-/microstructures. SEM images of LaOCl:Eu^{3+} nanofiber, nanotube and microbelt phosphors are also shown in (**a**). **b** The CL spectra of LaOCl:Eu^{3+} phosphors with fiber, tube, and belt-like morphologies. **c** The CL photos of LaOCl:RE^{3+} (RE = Sm, Eu, Tb, Dy, Tm) 1D nanomaterials. The dependence of CL intensities of LaOCl:RE^{3+} 1D nanomaterials of **d** accelerating voltage (kV) and **e** filament current (mA). Adapted from Ref. [40] by permission of Wiley

morphologies/sizes is shown in Fig. 2.5b, and it can be seen that the belt-like sample has a higher CL intensity than that of fiber-like and tube-like samples. This is because that the LaOCl:Eu^{3+} nanofibers and nanotubes produce more surface defects than microbelts due to smaller nanoparticles and larger surface area. However, defects have serious drawback for luminescent intensity of phosphors as they provide non-radiative recombination routes for electrons and holes. The same morphology- and size-dependent luminescence performance appears in systems of $LaPO_4$:Ce^{3+}/Tb^{3+} [64], YVO_4:RE^{3+} (RE = Eu, Tb, Dy, Sm) [65], $CaWO_4$:Tb^{3+} [19], and so on. Therefore, controllable modification of morphology and size of 1D luminescent materials can elevate their luminous efficiencies. Via the electrospinning process, RE^{3+} (Eu^{3+}, Tb^{3+}, Tm^{3+}, Sm^{3+}) can be homogenously dispersed in LaOCl systems and the luminescence colors can be tuned in a wide range through changing RE^{3+} concentrations and codoping RE^{3+} ions (Eu^{3+}/Tb^{3+}, Eu^{3+}/Tm^{3+}, Eu^{3+}/Tb^{3+}/Tm^{3+}) as shown in Fig. 2.5c. In addition, the increase in CL intensity (brightness) with an increase in electron energy and filament current are attributed to the deeper penetration of the electrons into the phosphor body and the larger electron beam current density. However, a larger current density may result in the accumulation of excess electrons on phosphor surface. If these electrons could not be promptly transferred, the cathodoluminescent efficiency will be reduced due to a saturation behavior. Under low-voltage electron beam excitation, the CL emission intensities of 1D LaOCl:RE^{3+} nanophosphors gradually elevate with raising

accelerating voltage and filament current without obvious saturation behavior (Fig. 2.5d, e), which is beneficial to apply in FED devices.

Hydrolysis Sol–gel method. According to the previous research, the emission performances can be improved in spherical phosphors with respect to the irregular ones, which are basically attributed to the high packing densities and low scattering of light [12, 56]. Therefore, there is a growing interesting on synthesizing inorganic phosphors with spherical morphologies in recent years [66]. As one of the most well-known hydrolysis method, Stöber method [67] that based on hydrolysis of tetraethylorthosilicate (TEOS) in an alcohol medium in the presence of water and ammonia has been extensively employed to prepare the monodisperse silica (SiO_2) spheres with different sizes from nano- to micron meter by a modified procedure. Some research groups developed a combination of these monodisperse SiO_2 spheres and the PSG process following suitable annealing temperatures to synthesize a series of monodisperse and spherical core–shell-structured phosphors [47]. The concrete experimental process is extremely simple as follows (Fig. 2.6): first, stir the as-formed SiO_2 particles in corresponding PSG precursor solutions of the phosphors (composing of metal ions, citric acid, and PEG) and then separate the SiO_2 particles by centrifugation following a heat treatment at certain temperature to obtain the final phosphor products. The size for the phosphor particles can be controlled by the ones of the silica cores and the number of coating cycles [66]. By the above method, a variety of precursor solutions of phosphors can be coated on the surface of SiO_2 spheres to form the desirable spherical phosphors. More important, the luminescent properties of core–shell-structured phosphor particles can be tuned and optimized by changing the size of SiO_2 cores and thickness of phosphor shells [68]. In summary, it is a general method to prepare spherical phosphors for almost all of the inorganic salt phosphors.

Spray pyrolysis process. Except for hydrolysis sol–gel method, other better morphology of the spherical shape with a size around 0.5–3 μm for phosphors can be obtained by the spray drying process [43]. It needs a combination of PSG precursor solutions and subsequent annealing process to obtain final phosphor products. By loading the corresponding precursor solution on a spray drying apparatus and a following annealing process at high-temperature (600–1200 °C),

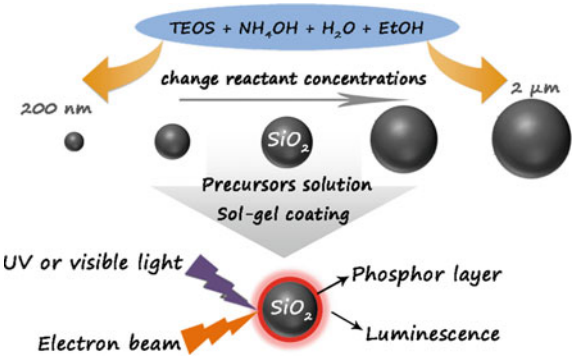

Fig. 2.6 Hydrolysis-Sol/gel synthesis of spherical core-shell-structured phosphors

the representative red-emitting $Y_2O_3:Eu^{3+}$ [47], red-emitting $CaTiO_3:Pr^{3+}$ [69], green-emitting $YBO_3:Tb^{3+}$ [70], and blue-emitting $Sr_2CeO_4:Ce^{3+}$ [43] FED phosphors were also prepared to spherical particles with sizes ranging from 0.6 to 3.0 μm. It is demonstrated that the as-prepared spherical phosphors indeed improve their emission intensity over the other irregular ones, which is also due to high packing densities and low scattering of light. It is noticed that the disadvantages of phosphors prepared by spray pyrolysis are that the optimal heating temperature was generally higher than that for the solid-state reaction. Moreover, it also has a bigger size distribution than that prepared by homogenous precipitation or hydrolysis Sol–gel methods. Therefore, it will be further improved.

2.2.2 *Modification of Phosphor Composition*

For phosphors, it frequently involves in the substitution of cations in host lattice with activator ions to produce luminescence, which easily results in a mismatch of charge and crystal lattice due to different valence state and ion radius. These mismatches will generate many defects (vacancy, gap, crystal lattice distortion, and strain) to decrease the luminescent efficiency of phosphors and as a result need to be avoided or reduced. By modifying phosphor composition, the luminescent performance of phosphors can be efficiently improved. Generally, composition modifications of phosphors mainly focus on two aspects: the one is to conduct charge compensations for relaxing charge mismatch, and the other one is to relieve crystal lattice strain by introducing other cations with complementary radius. Based on the above consideration, representative $Ca_2GeO_4:Eu^{3+}$ and $Zn_2GeO_4:Mn^{2+}$ phosphors have been optimized, and the effect of composition modification on cathodoluminescent efficiencies of phosphors has been elaborately investigated. In Mg-doped $Zn_{1.96}GeO_4:0.04Mn^{2+}$ systems, it shows the maximum emission at 532 nm under the excitation of 3 kV accelerating voltage, which corresponds to the characteristic emission of Mn^{2+} from $^4T_1$ to $^6A_1$. The CL intensity increases with the replacement of Mg^{2+} ions. The possible reason is the join of Mg^{2+} ions (r = 0.57 nm, and coordination number (CN) = 4) decreases the crystal lattice strain due to mismatched ions radius with Zn^{2+} (r = 0.60 nm, CN = 4) and Mn^{2+} (r = 0.66 nm, CN = 4) ions. The relaxing of crystal lattice strain can efficiently suppress non-radiative processes and finally result in the improvement of cathodoluminescent efficiency [20]. For $Ca_{1.99}GeO_4:0.01Eu^{3+}$ systems, there is a charge mismatch between Eu^{3+} and Ca^{2+} ions. According to the electroneutrality theory, two Eu^{3+} ions will replace three Ca^{2+} ions to obtain charge balance, and as a result, two positive defects of $[Eu_{Ca}]^{\bullet}$ and one negative Ca^{2+} vacancy of $[V_{Ca}]''$ would form. These defects and vacancies may capture excited electron to proceed to non-radiative transitions and damage the luminous efficiency. Codoping Li^+ ions can help to incorporate the Eu^{3+} ions into Ca^{2+} sites by compensating for the different charges between Eu^{3+} and Ca^{2+} ions, and the red light emission intensity of $Ca_{1.98}Li_{0.01}Eu_{0.01}GeO_4$ is elevated with respect to $Ca_{1.99}Eu_{0.01}GeO_4$ [72].

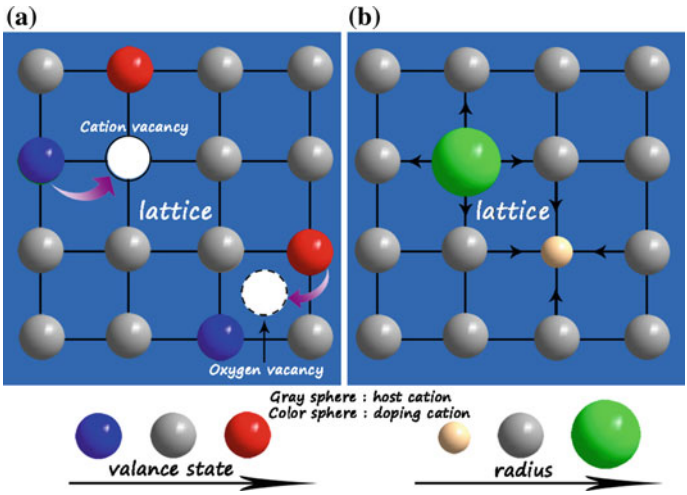

Fig. 2.7 A simple model to illustrate the possible increasing mechanism of luminescent efficiency by composition modification (charge compensations and crystal lattice strain relaxing)

A simple model to illustrate the possible increasing mechanism of luminescent efficiency by composition modification is shown in Fig. 2.7. During the process of doping cations into host lattice, if its valence state is higher than that of host cations, cation vacancies will be produced, whereas oxygen vacancies will appear (Fig. 2.7a). These vacancies, namely crystal lattice defects, increase the probability of non-radiative transitions and thus decrease luminescent efficiency. When introducing charge compensator ions into the host lattice, it will reduce charge defects and thus can improve luminescent performance. On the other hand, cationic replacements with different radius in one matrix will result in crystal expansion or shrinkage. This will generate strain or many defects due to the distorted crystal lattice, which also increases the possibility of non-radiative transitions. By doping other ions with complementary radius, it can relieve lattice strain and then decrease defects, which finally enhance luminescence efficiency of phosphor (Fig. 2.7b). In general, the cathodoluminescent efficiency of FEDs phosphors can be optimized by composition modification including charge compensations and crystal lattice strain relaxing, which promotes a potential application of phosphors in FED devices.

2.2.3 Improvement of Conductivity

It is well known that electron beam is used as excitation source in FED technology. In order to realize highly efficient FED, phosphors should be efficiently excited by low-voltage electrons. Although the accelerating voltage employed in FEDs is much less than that worked in CRTs, its energy is still much higher than UV or

visible light radiation, which is around a few thousand to thousands of eV [71]. If could not be promptly transferred, these electrons very easily accumulate on the phosphor surface to recombine with holes/surface defects, which increase non-radiative transitions and thus decrease cathodoluminescent efficiency. In addition, excessive electrons staying on the phosphor surface also easily reach charge saturation. The tendency for the brightness to plateau even when the current is increased at a fixed electron voltage; this is a serious concern especially for FEDs since the voltage is normally low (<4 kV). Requiring high current for high power and brightness. Accordingly, an important question for FEDs is how to eliminate or weaken charging and surface recombination effects, and improve the saturation. One of the most promising and efficient approach is to improve the conductivity of FED phosphors. This approach can efficiently and opportunely release the accumulated charges on phosphors and thus improve the saturation of phosphors and enhance their cathodoluminescent efficiency. Generally, there are two main routes to increase the conductivity of FED phosphors: the one is the selection of semiconductor materials as host lattice, and the other one is to mix transparent and conductive nanocrystalline powders with FED phosphors. For the selection of hosts, it is known that the compounds composed of elements with small differences in electronegativity should have a narrower band gap [72]. Moreover, the band gap of oxide-based phosphor systems is related to crystal structures of hosts [23, 38]. Generally, reticular acid radical-coordinated polyhedrons in host easily result in a narrow band gap of host. While the band gap of host has great effects on the conductivity and luminescent efficiency of phosphors. A narrow gap can lead to higher conductivity which is beneficial to the cathodoluminescence. On the other hand, luminescence quenching will occur if the energy levels of excited states of activator ions are located among the conduction band of host. Only the excited states of activator ions locate below the conduction band of host, the phosphors present excellent luminescent performance. Therefore, appropriate hosts with reasonable band gap should be considered during the exploration and design of novel FED phosphors, which could merge the luminescence performance and conductivity of phosphors. According to the first route, a series of RE^{3+} ions or Mn^{2+} ions activate Ga_2O_3 [32], $(Ca,Sr)In_2O_4$ [35, 36], $La(Ga,In)O_3$ [49], $Mg_2(Sn,Ti)O_4$ [30], $(Zn,Mg)_2GeO_4$ [38], Li_2ZnGeO_4 [20]. FED phosphors were derived, as summarized in Table 2.1. Except for the efficient transport of electrons, semiconductor hosts (emission from UV to bluish-green light region) generally have a sensitive enhancement for luminescent efficiency of RE^{3+} ions.

Another route toward increasing phosphor conductivity is a mixing of conductive nanocrystalline powders like In_2O_3, SnO_2, ZnO, and Au [12, 33, 73–75]. Zhang et al. [76] encapsulated In_2O_3 layer on $Y_2O_3:Eu^{3+}$ phosphor particles and concluded positive effect on the cathodoluminescent performance. They found that the luminous efficiency of $Y_2O_3:Eu^{3+}@In_2O_3$ phosphor screens was obviously improved with respect to uncoated $Y_2O_3:Eu^{3+}$, as shown in Fig. 2.8a. Moreover, the luminous efficiency of the former improves much more than the latter with an increase in the accelerating voltage. This is attributed to the increased electrical conductivity of $Y_2O_3:Eu^{3+}$ phosphors with increasing In_2O_3 coating. In_2O_3-coated

Table 2.1 CIE chromaticity coordinates, emission colors of color gamut enlarged phosphors under low-voltage electron beam excitation

Sample	Color coordinates	Color	Refs.
$Mg_{2(1-y)}Sn_{(1-x)}O_4$: x% Ti^{4+}, y% Mn^{2+}			
x = 2.0, y = 0.01	(0.1637, 0.2574)	Cyan	[30]
Li_2CaSiO_4:Eu^{2+}	(0.119, 0.203)	Cyan	[85]
$BaZrSi_3O_9$:Eu^{2+}		Cyan	[86]
$BaSi_2O_2N_2$:Eu^{2+}		Cyan	[87]
$NaCaPO_4$:Mn^{2+}	(0.428, 0.552)	Yellow	[51]
$LaGaO_3$:0.5 %Sm^{3+}	(0.4880, 0.4153)	Yellow	[71]
$ZnGeN_2$		Yellow	[7]
$LaAlO_3$:0.25 %Sm^{3+}	(0.5133, 0.4625)	Yellow	[48]
$Ca_2Gd_8(SiO_4)_6O_2$:5 %Ce^{3+}, 25 %Mn^{2+}	(0.545, 0.415)	Yellow	[88]

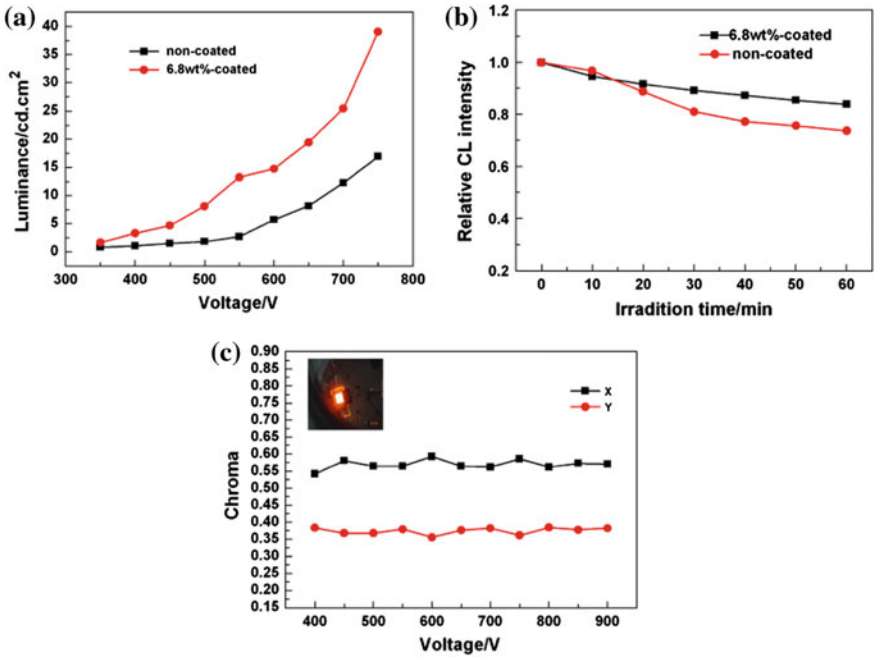

Fig. 2.8 **a** Dependence of luminous efficiency of Y_2O_3:Eu^{3+} phosphor screens before and after In_2O_3 coating on the excitation voltage. **b** Comparison of the relative CL degradation behavior and of uncoated and In_2O_3-coated Y_2O_3:Eu^{3+} phosphor screens. **c** The variation of chromaticity of In_2O_3-coated phosphor screen with an accelerating voltage. The *inset* shows a macrophotograph of the Y_2O_3:Eu^{3+} phosphors coated with 6.8 wt% In_2O_3 on excitation at 700 V. Adapted from Ref. [76] by permission of Wiley

Y_2O_3:Eu^{3+} phosphor screens have a better stability than uncoated one under 700 V accelerating voltage (Fig. 2.8b). This is because that the conductive In_2O_3 nanoparticles not only can reduce surface charge accumulation but also may serve as protective layer on phosphor surface to prevent chemical degradation caused by the direct electron beam bombardment. Finally, the aging rate of the low-voltage CL efficiency is suppressed, and as a result, the lifetime and stability of the phosphor screens are improved evidently. In addition, the Commission International del'Eclairge (CIE) chromaticity coordinate values of Y_2O_3:Eu^{3+}@In_2O_3 phosphors are nearly invariable (x and y keeps at about 0.575 and 0.375) with changing accelerating voltage (Fig. 2.8c), maintaining a color stability. The similar improvement for cathodoluminescent efficiency and luminance appears in In_2O_3-coated $ZnGa_2O_4$ and $ZnGa_2O_4$:Mn^{2+} phosphors [73, 74]. Therefore, employing some conductive materials on the surface of phosphor indeed can reduce the accumulated electrons on the surface of phosphor and improve the cathodoluminescent efficiency of phosphors. This may also act as a bridge to drain the Coulomb charge to the ITO substrate efficiently, which decreases the excited voltage and improves the lifetime, stability, and efficiency of the phosphor screen.

2.2.4 Improvement of Electron-Stimulated Degradation Behavior

It is known that most phosphors will degrade upon exposure to large doses of electrons (>50 C/cm^2). The luminescent degradation property of phosphors under electron beam bombardment is very important for their FED application. The origin of this degradation is now becoming clear, which is generally considered to be related to the stability of crystal structures and electron-stimulated surface chemical reaction of phosphor grains [78, 79]. Because prolonged electron beam irradiation commonly can decompose phosphors into volatile atomic species through the surface chemical reaction and then a possible formation of new layers on the surface. While the decomposition and hence the formation of the new layers has negative effects on both the chemical stability and luminescent intensity of the FEDs phosphors. To prevent the phosphors from decomposition, two strategies can be employed: first, selecting hosts with excellent chemical stability under electron beam irradiation; second, coating Al_2O_3, In_2O_3, ZnO, SiO_2, BN and organic polymers on phosphor surface [80]. The formers require stable crystal phases and crystal structures for phosphors, which can endure continuous electron beam irradiation. The rare earth ion-activated semiconductor materials and (oxo)nitridosilicates are possible selections [81]. The use of coatings can also yield excellent stability to the phosphors when exposed to moisture and other atmospheric components, and to protect phosphors from irradiation damage. For example, Xu et al. [33] investigated the degradation properties after mixing the representative $Lu_3Ga_5O_{12}$:Tb^{3+} phosphor with In_2O_3 nanoparticles. Figure 2.9a shows that the

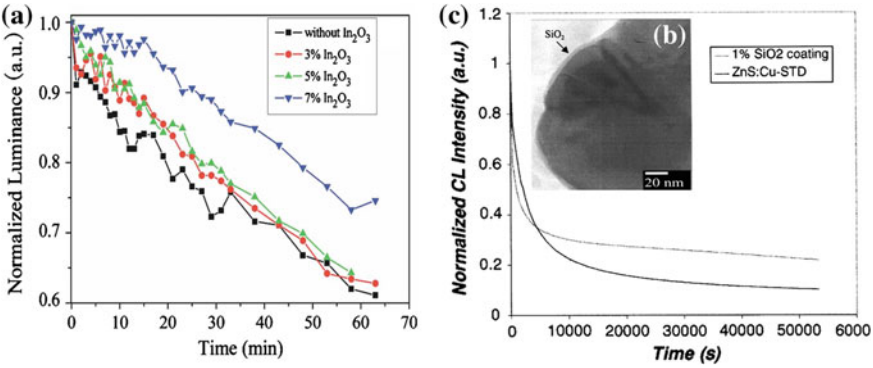

Fig. 2.9 **a** Normalized luminance decay of $Lu_3Ga_5O_{12}:Tb^{3+}$ phosphor mixed with and without In_2O_3 nanoparticles as a function of bombardment time. **b** TEM cross-sectional micrographs of 1.0 wt% SiO_2-coated ZnS:Cu phosphors. **c** Normalized CL intensity at 2 kV of 1.0 wt% SiO_2-coated and uncoated ZnS:Cu phosphors as a function of time. **a** Adapted from Ref. [33] by permission of American Vacuum Society. **b**, **c** Adapted from Ref. [77] by permission of The Electrochemical Society

degradation of the phosphor film becomes slow after being mixed with In_2O_3. Moreover, it becomes slower with increasing In_2O_3 contents. The decay is partially due to the charge-up of the phosphor. The improvement of the conductivity of $Lu_3Ga_5O_{12}:Tb^{3+}$ phosphor film by mixing with In_2O_3 eases the charge-up effect, and thus, the slower decay can be observed. After stopping bombardment for a while, however, the luminance could not restore to the initial value, indicating besides the charge-up effect, permanent damage to the phosphor occurs. This may be due to the accumulation of carbon at the surface during electron bombardment. This carbon contamination will prevent low-energy electrons from reaching the phosphor grains and also exacerbate surface charging, and thus lower the luminance. In addition to the mixing with semiconductive materials, Do et al. confirmed that coating SiO_2 on phosphor surface can also efficiently improve their electron-stimulated stability [82]. Figure 2.9b shows the formation of thin and uniform coatings on ZnS:Cu powders with a thickness of 5 nm. They founded that the SiO_2-coated phosphors were far more resistant to the loss of S species and to the formation of oxide dead layer. The CL aging study (Fig. 2.9c) showed much improved CL efficiency curves for the coated phosphors, confirming that the encapsulation of thin and uniform SiO_2 coatings on ZnS:Cu served as protective layers retarding the surface-related degradation, which is critically important for the development of commercial FEDs. On the other hand, the surface protective species need not necessarily be always externally applied, they can also originate from electron-stimulated surface chemical reaction [78]. This is attributed to surface disassociates partially of a phosphor compound. Pitale et al. found that a thermodynamically stable Al_2O_3 layer could be formed on the surface of lithium aluminate family like $LiAl_5O_8$:Tb as a result of the electron-stimulated surface chemical reactions [78, 82]. Moreover, it generates a positive contribution to the CL stability

of the $LiAl_5O_8$:Tb phosphor. In general, the stable crystal structures and the surface protective species indeed can enhance the time stability of phosphors under electron beam irradiation to some extent. It is noticed that although the improvement can simply attribute to electron-stimulated surface chemical reaction, the more exact degradation mechanism is not clear and need to be further studied.

2.2.5 *Enlarge Color Gamut*

The resolution is a vital parameter for display devices, which is strongly related to the color gamut of phosphor [12, 40]. Generally, the wider of color gamut of phosphor, the higher picture quality can be achieved. The typical color gamut for FEDs is made up of a triangle region enclosed by three chromaticity coordinate points of trichromatic (red, green, and blue, RGB) FED phosphors, (0.647, 0.343) ($Y_2O_2S:Eu^{3+}$; red), (0.298, 0.619) (ZnS:Cu,Al; green), and (0.146, 0.056) (ZnS:Ag, Al; blue). In order to realize high-quality full-color FEDs, it is necessary to enlarge the color gamut of these phosphors. There are two main strategies to reach this goal. The one is to develop FED phosphors with higher color purity with respect to current trichromatic FED phosphors. The other one is to explore some novel phosphors with their CIE chromaticity coordinates locating out of the above triangle area. According to the first strategy, a series of RGB phosphors with high color purity have been developed. For example, blue-emitting Tm^{3+}-doped La_2O_3, LaOCl, LaOF, $LaGaO_3$, and so on were prepared and investigated [41, 49, 59, 71]. These phosphors demonstrate more higher color purities than commercial FED blue phosphor Y_2SiO_5:Ce due to main $^1D_2$–$^3F_4$ (around 458 nm) transition emission of Tm^{3+} ions (Table 2.1). Some Tb^{3+}-activated phosphors such as Tb^{3+}-doped LaOCl, $LaGaO_3$, and $KNaCa_2(PO_4)_2$ can also give highly pure blue emission through a low Tb^{3+} doping content due to the main $^5D_3$–$^7F_{6\text{-}0}$ transitions [83]. For these 4*f*–4*f* transitions of RE ions, the emission spectra are narrow and the peak positions are basically stable in different hosts because the electrons in 4*f* orbits are strongly shielded by the outside 5*s* and 5*p* electrons. As a result, they can maintain a high color purity. However, for 5*d*–4*f* transitions of RE ions, the energy level of the excited state $4f^{n-1}5d$ is commonly lower than that of the lowest excited state, which generally presents a broadband emission. Due to the bare electrons in 5*d* states, the different coordination surroundings of hosts have a prominent influence on the luminescence of RE ions, which can tune the emission colors from ultraviolet to red light region. For example, Hirosaki et al. [84] reported a highly pure blue emission of Eu^{2+} in AlN host with CIE coordinate (0.139, 0.106). Under electron beam excitation, it showed better saturation behavior, brightness, and degradation behavior than that of Y_2SiO_5:Ce. So it is an excellent blue-emitting FED phosphor. Mn^{2+} is a transition metal ion with $3d^5$ electronic configuration, and its emission, corresponding to $^4T_1 \rightarrow {}^6A_1$ transition, consists of a broad band whose position depends strongly on the host lattices. If the crystal field around Mn^{2+} ion is weak, the splitting of the excited energy levels in 3d orbits will be small resulting in Mn^{2+}

emission with higher energy, whereas it will give lower energy emission. Due to the weak crystal field surroundings, the as-prepared Mn^{2+}-activated Mg_2SnO_4, $(Zn, Mg)_2GeO_4$ and Li_2ZnGeO_4 phosphors give Brilliant green emission with narrow band width, which makes them have higher green purity than commercial green ZnO:Zn phosphors (Table 2.1). Therefore, they are promising green-emitting FED phosphors, while $Mg_2Y_8(SiO_4)_6O_2:Ce^{3+}/Mn^{2+}$ and $Ca_4Y_6(SiO_4)_6O:Ce^{3+}/Mn^{2+}$ show excellent red emission of Mn^{2+} due to the strong crystal field surroundings, which can be used for highly efficient red-emitting FED phosphors. Other promising red-emitting phosphors like $Ca_2GeO_4:Eu^{3+}$ and $CaTiO_3:Pr^{3+}$ also have potential application in FEDs due to high color purity (Table 2.1) [63, 72]. In general, developing phosphors with higher color purity than commercial RGB FED phosphors is a feasible strategy to improve display quality.

On the other hand, the colors observed by the human eye are those depicted in the whole 1931 CIE chromaticity diagram according to the colorimetry theory. At a four-color system, if four points are selected as red, yellow, green, and blue (RYGB) or red, green, cyan, and blue (RGCB), they would surround a larger color gamut than the three-color system [7, 71]. Therefore, these four-color systems will display more natural color than RGB system, and thus better meet people's individual requirements. Moreover, four-color system has a higher "information density" (namely, the pixels per unit area) compared with three-color system. Accordingly, the second strategy to enhance the display quality is to explore suitable four-color (RYGB) or (RGCB) systems phosphors such as cyan- or yellow-emitting phosphors. As mentioned in the previous section, the emission of Eu^{2+} ion can vary from ultraviolet to red light which depends on the host lattice. Therefore, Eu^{2+} ion can obtain cyan emission by selecting suitable host. Xie and Wang et al. realized cyan emission of Eu^{2+} ions in $Li_2CaSiO_4:Eu^{2+}$ [85] and $BaZrSi_3O_9:Eu^{2+}$ [86] systems, respectively, as shown in Table 2.1. Eu^{2+}-activated $BaSi_2O_2N_2$ can also be developed as cyan-emitting FED phosphor due to its excellent stability and high color purity (Table 2.1) [87]. In addition, Li et al. designed a highly pure cyan light emission by mixing blue light (Ti^{4+}) and green light (Mn^{2+}) in Ti^{4+}, Mn^{2+}-codoped Mg_2SnO_4 system, as shown in Fig. 2.10a, b. The as-prepared cyan-emitting phosphors have good stability under low-voltage electron beam excitation. After continuous electron beam excitation for an hour, it still keeps 92 % of its original intensity, with little change in their CIE chromaticity coordinates [30]. Therefore, it is promising phosphor for use in FEDs. Based on the second strategy, $NaCaPO_4:Mn^{2+}$ shows bright yellow emission under electron beam excitation with the CIE chromaticity coordinate (0.428, 0.552), which has a higher color purity than commercial yellow-emitting FED phosphor $(Zn, CdS):Ag^+$, as shown in the inset of Fig. 2.10c, d [51]. Under different voltages and continuous electron beam bombardment, its CIE chromaticity coordinates present a good stability. Moreover, there is no obvious saturation effect for the CL intensity of these phosphors with the increase in V_a and J_a. So the as-prepared $NaCaPO_4:Mn^{2+}$ phosphors have potential to be used as yellow-emitting phosphor in four-color system (RGBY) FEDs. Other yellow-emitting $ZnGeN_2$ [7], $LaAlO_3:Sm^{3+}$ [48], $LaGaO_3:Sm^{3+}$ [71], and $Ca_2Gd_8(SiO_4)_6O_2:Ce^{3+}/Mn^{2+}$ [88] also demonstrate

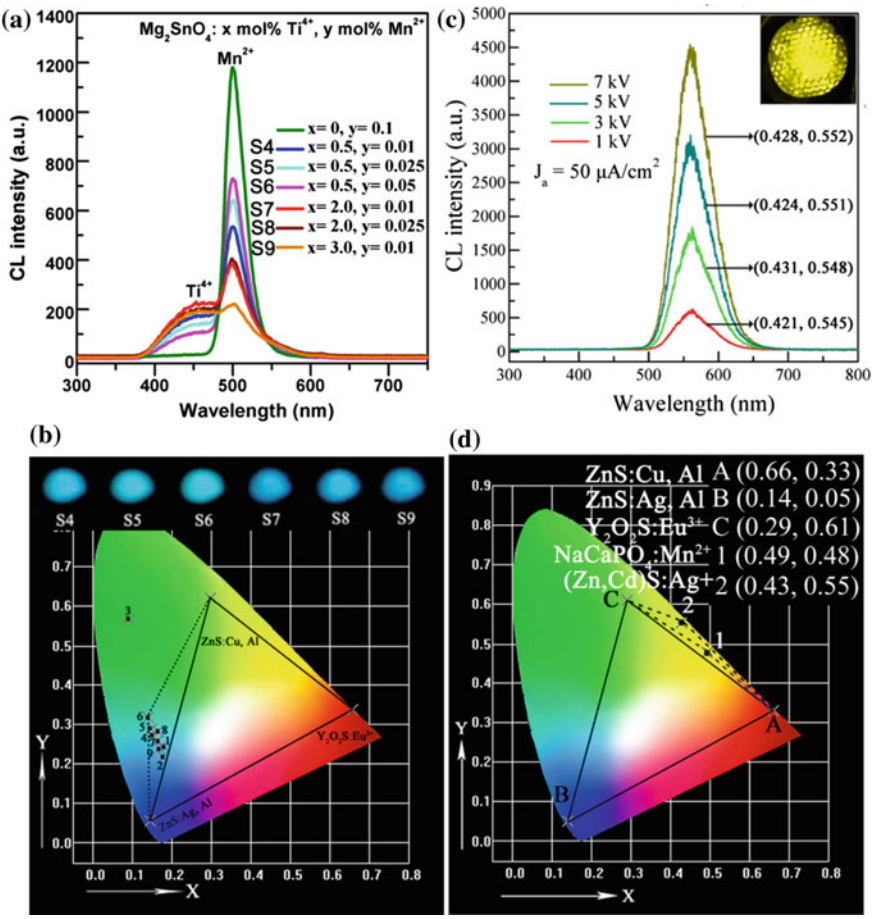

Fig. 2.10 CL spectra of **a** Mg_2SnO_4:xTi^{4+}, yMn^{2+} (x = 0–0.03, y = 0.0001–0.001) and **c** $NaCaPO_4$:0.03Mn^{2+} samples. The CIE chromaticity coordinates of **b** Mg_2SnO_4:xTi^{4+}, yMn^{2+} (x = 0–0.03, y = 0.0001–0.001) and **d** $NaCaPO_4$:0.03Mn^{2+} samples. The *triangle* and *quadrangle* in **b** and **d** show the typical and enlarged color gamut for FEDs phosphors, respectively. The *insets* in **b** and **c** are cathodoluminescent photographs. **a**, **b** Adapted from Ref. [30] by permission of Royal Society of Chemistry. **c**, **d** Adapted from Ref. [51] by permission of Optical Society of America

excellent chromaticity coordinates and stability (Table 2.1), which are also potential RYGB system phosphors in FED devices. In general, the development of highly pure RGB phosphors and appropriate four-color system (cyan or yellow-emitting phosphors) phosphors can efficiently enlarge color gamut and improve color saturation, and further to realize high-quality FED.

2.2.6 Design of White Light Emission

It is well known that excellent white light emission can supply excellent backlights in the display fields like LED, LCD, PDP, and FEDs, which has a positive effect on display quality. In recent years, there is an increasing focus on obtaining white light emission in single-phase host due to some potential advantages in luminous efficacy, chromatic stability, color-rending index, and cost against the mixing of two or three different phosphors [89]. Many excellent and tunable white-light-emitting materials for FEDs can be obtained via designing co-emission (mono- or codoping RE^{3+} ions) and energy transfer (from hosts or RE ions to RE ions or Mn^{2+} ions) in single-phase hosts. The basic guiding principle mainly involves in a complex of complementary luminescence such as blue and yellow light, red, green, and blue light to obtain white light emission. A schematic illustration of generation of white light via co-emission and energy transfer in single-phase host is shown in Fig. 2.11. Due to abundant emission colors from blue to red based on 4*f*–4*f* transitions of trivalent RE^{3+} ions, white light emission in co-emission systems can be realized through mono-doping Eu^{3+} or Dy^{3+} ions, and codoping Tm^{3+}/Dy^{3+}, Tb^{3+}/Sm^{3+}, Tb^{3+}/Eu^{3+}, $Tm^{3+}/Tb^{3+}/Eu^{3+}$ ions, etc., into single matrix (Fig. 2.11a), while white light emission in energy transfer systems mainly results from the $Ce^{3+} \rightarrow Mn^{2+}$ (blue–yellow light complex) and $Ce^{3+} \rightarrow Tb^{3+}$, Mn^{2+} (red–green–blue light complex) energy transfers, as shown in Fig. 2.11b. The summary of luminescent properties for single-phase white-emitting phosphors via co-emission and energy transfer under low-voltage electron beam excitation is shown in Table 2.2. It is noticed that the energy can also be transferred to the lower energy excited state among the RE ions, depending on the RE concentration, energy transfers rates, and phonon energy. Moreover, the more energy transfer occur among the RE ions, the lower the luminescence efficiency. Therefore, it is important to optimize RE ion-doping concentrations and select suitable hosts. The elaborate discussions are shown as follows.

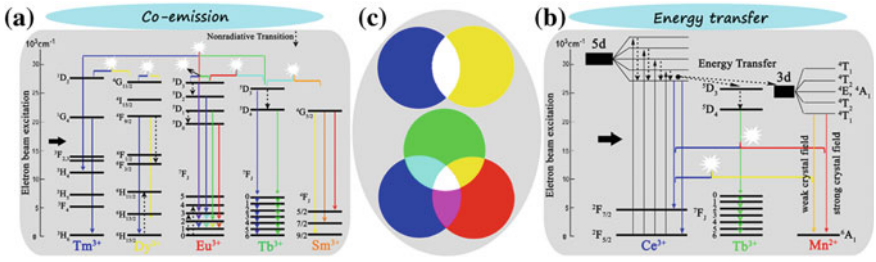

Fig. 2.11 Schematic mechanisms of generation of white light via **a** co-emission (mono-/codoping RE^{3+} ions) and **b** energy transfer (from hosts or RE ions to RE ions or Mn^{2+} ions) in single-phase host. **c** A generation of white light through the complex of different colors, *Blue-Yellow* (BY) or *Red–Green–Blue* (RGB). *Colored straight lines with arrows* represent different luminescence. The *horizontal braces* with different colors represent different light emission and *white stars* represent white light by the complex of different light emission

1. Singly doping RE^{3+} ions like Eu^{3+} or Dy^{3+} into appropriate single host.

The trivalent Eu^{3+} ion is well known as a red-emitting activator due to its $^5D_0$–^7F_J transitions based on $4f^6$ configuration with the most prominent $^5D_0$–$^7F_2$ emission group around 610–625 nm [35]. Except for the essential red emission, some other emission lines located in blue-green region from higher ^5D levels, such as $^5D_1$ (green), $^5D_2$ (green, blue), and $^5D_3$ (blue) can also appear at the low phonon frequencies of the host lattices and the low doping concentration of Eu^{3+} (Fig. 2.11a). That is attributed to the avoidance of the multiphonon relaxation and cross-relaxation occurring among the energy levels of Eu^{3+}, respectively. If the phonon energy (highest vibration frequency, ν_{max}) of the host lattice is high enough to cause multiphonon relaxation, it will quench the higher-level $^5D_{1,2,3}$ emission of Eu^{3+}. Moreover, if the doping concentration of Eu^{3+} is high, the $^5D_{1,2,3}$ emission might be quenched by cross-relaxation between two neighboring Eu^{3+} ions, such as Eu^{3+} ($^5D_1$) + Eu^{3+} ($^7F_0$) → Eu^{3+} ($^5D_0$) + Eu^{3+} ($^7F_3$) and Eu^{3+} ($^5D_3$) + Eu^{3+} ($^7F_0$) → Eu^{3+} ($^5D_2$) + Eu^{3+} ($^7F_4$). So whether the emission can occur from higher excited states $^5D_1$, $^5D_2$, and $^5D_3$ or not for Eu^{3+} ion depends critically upon the highest vibration frequencies (ν_{max}) available in the host lattice and the doping concentration of Eu^{3+}. In other words, an appropriate selection of the host lattice and doping concentration of Eu^{3+} is possible to yield simultaneously the red emission from $^5D_0$ energy level and the blue and green emissions from the higher $^5D_{1,2,3}$ energy levels of Eu^{3+} with comparable intensity, thus generating a white light emission from Eu^{3+}-monodoped materials. This situation has been confirmed in Eu^{3+}-doped $CaIn_2O_4$ system. Under low-voltage electron beam excitation, the emission spectra of $CaIn_2O_4$:0.01Eu^{3+} consist of all the emission lines from the $^5D_{0,1,2,3}$ excited states to the ^7F_J ground states of Eu^{3+}, i.e., $^5D_3$–$^7F_1$ (418 nm), $^5D_3$–$^7F_2$ (431 nm), $^5D_3$–$^7F_3$ (447 nm), $^5D_2$–$^7F_0$ (467 nm), $^5D_2$–$^7F_2$ (492 nm), $^5D_2$–$^7F_3$ (512 nm), $^5D_1$–$^7F_1$ (537 nm), $^5D_1$–$^7F_2$ (555 nm), $^5D_0$–$^7F_1$ (588 nm), $^5D_0$–$^7F_2$ (616 nm), and $^5D_0$–$^7F_4$ (700 nm), as shown in Fig. 2.12a. These emission lines of Eu^{3+} cover the whole visible spectral region and have comparable intensities resulting in a brilliant white light emission. Moreover, tunable white light emission can be obtained by precisely controlling the doping concentration of Eu^{3+} ions, as shown in Table 2.2. According to the same approach, $LaInO_3$:Eu^{3+}, LaOF:Eu^{3+} and β-$NaYF_4$:Eu^{3+} have been developed as single-phase white-light-emitting FEDs phosphors (Table 2.2) [90].

For Dy^{3+} ions, its emission spectrum is mainly separated into two groups, the blue emission from 460 to 505 nm and the yellow emission from 570 to 600 nm accompanied by a group of weak lines in the red region from 650 to 700 nm based in its $4f^9$ configuration. These emissions correspond to the transitions from $^4F_{9/2}$ to $^6H_{15/2}$, $^6H_{13/2}$ and $^6H_{11/2}$ of Dy^{3+} (Fig. 2.11a), respectively [74]. The yellow-emitting $^4F_{9/2}$–$^6H_{13/2}$ transition is hypersensitive transition, which is susceptible to the crystal environment. However, the blue emission is basically invariant with the surrounding environment. In composite oxides, the covalency between Dy^{3+} and O^{2-} has an important effect on the ratio of yellow-to-blue emission. Generally, the bigger covalency, the stronger yellow emission of Dy^{3+}

Table 2.2 Summary of cathodoluminescent properties for single-phase white-emitting phosphors via co-emission and energy transfer systems

Phosphor	Emission peaks (nm)/Transitions/Colors	CIE (x, y)	Refs.
Monodoping systems			
$CaIn_2O_4$:0.5 %Eu^{3+}	All the emissions from Eu^{3+}: ^5D_J–$^7F_{J'}$ $^5D_0$–$^7F_{J'}$, orange-red; $^5D_1$–$^7F_{J'}$, green $^5D_2$–$^7F_{J'}$, green-blue; $^5D_3$–$^7F_{J'}$, blue (J = 0, 1, 2, 3; J' = 0, 1, 2, 3, 4)	(0.290, 0.310)	[26]
$CaIn_2O_4$:1 %Eu^{3+}		(0.324, 0.323)	
$CaIn_2O_4$:1.5 %Eu^{3+}		(0.358, 0.345)	
$LaInO_3$:0.5 %Eu^{3+}		(0.369, 0.404)	[90]
LaOF:0.2 %Eu^{3+}		(0.291, 0.340)	[59]
$SrIn_2O_4$:1.5 %Dy^{3+}	491, 580/$^4F_{9/2}$ to $^6H_{15/2}$, blue; $^6H_{13/2}$, yellow	(0.302, 0.329)	[36]
Ga_2O_3:3 %Dy^{3+}	492, 580/$^4F_{9/2}$ to $^6H_{15/2}$, blue; $^6H_{13/2}$, yellow	(0.299, 0.333)	[32]
Codoping systems			
LaOCl:Tm^{3+},Dy^{3+}	458/$^1D_2$–$^3F_4$ (Tm^{3+}), blue 480, 571/$^4F_{9/2}$ to $^6H_{15/2}$, $^6H_{13/2}$ (Dy^{3+}), yellow	(0.318, 0.329)	[41]
LaOCl:Tb^{3+},Sm^{3+}	384, 417, 438, 486, 543/$^5D_{3,4}$–$^7F_{6\text{-}2}$ (Tb^{3+}), bluish green 565, 607, 650/$^4G_{5/2}$–$^6H_{5/2,\ 7/2,\ 9/2}$ (Sm^{3+}), orange	(0.341, 0.321)	[83]
$LaGaO_3$:Tb^{3+},Sm^{3+}	414, 437/$^5D_3$–$^7F_{5,4}$; 414, 437/$^5D_4$–$^7F_5$ (Tb^{3+}), bluish green 561, 597, 642/$^4G_{5/2}$–$^6H_{5/2}$, $^6H_{7/2}$, $^6H_{9/2}$ (Sm^{3+}), yellow	(0.341, 0.334)	[71]
LaOCl:Tb^{3+},Eu^{3+}, Tm^{3+}	416, 438, 543, 486/$^5D_{3,4}$–$^7F_{6\text{-}4}$ (Tb^{3+}), bluish green 577, 594, 615/$^5D_0$–$^7F_{0,1,2}$ (Eu^{3+}), red 458/$^1D_2$–$^3F_4$ (Tm^{3+}), blue	(0.291, 0.312)	[40]
Energy transfer systems			
$Mg_2Y_8(SiO_4)_6O_2$: Ce^{3+},Mn^{2+},Tb^{3+}	425, 455/$5d^1$–$4f^1$(Ce^{3+}) blue; 613/$^4T_1$–$^6A_1$ (Mn^{2+}) red; 544/$^5D_4$–$^7F_5$ (Tb^{3+}), green	(0.332, 0.337)	[91]
$Ca_2Ca_8(SiO_4)_6O_2$: Ce^{3+},Mn^{2+}	403, 428/$5d^1$–$4f^1$(Ce^{3+}) blue; 590/$^4T_1$–$^6A_1$ (Mn^{2+}) yellow	(0.342, 0.318)	[88]
$Sr_3In(PO_4)_3$:Ce^{3+}, Mn^{2+}	375/$5d^1$–$4f^1$(Ce^{3+}) blue; 568/$^4T_1$–$^6A_1$ (Mn^{2+}) yellow	(0.331, 0.319)	[96]
$Ca_3Sc_2Si_3O_{12}$:Ce^{3+}, Mn^{2+}	450, 505/$5d^1$–$4f^1$(Ce^{3+}) blue to green; 574, 680/$^4T_1$–$^6A_1$ (Mn^{2+}) red		[97]

ion will be achieved. Moreover, the covalency of Dy^{3+}–O^{2-} is different in different host matrix due to the local variation of the symmetry and coordination environment of crystal structure. Therefore, the ratio of yellow-to-blue emission can be adjusted by doping into different host lattice, resulting in a possible to obtain white light emission in Dy^{3+}-monodoped luminescence material. For example, for

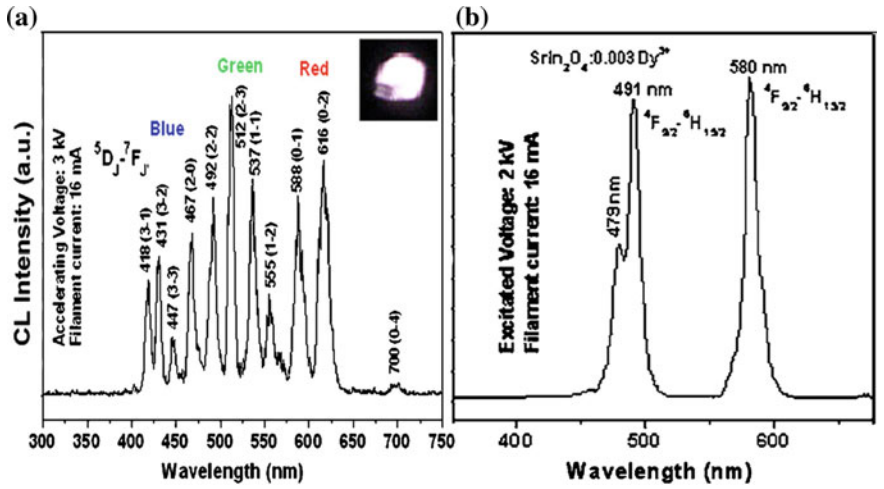

Fig. 2.12 Emission spectrum of **a** $CaIn_2O_4$:0.01Eu^{3+} under the excitation of electron beam. The *inset* shows luminescent photograph with white light emission. **c** Typical cathodoluminescence spectra of $SrIn_2O_4$:0.003Dy^{3+} with CIE chromaticity coordinates $x = 0.3019$ and $y = 0.3291$. **a** Adapted from Ref. [26] by permission of American Institute of Physics. **b** Adapted from Ref. [36] by permission of The Electrochemical Society

$SrIn_2O_4$:0.015Dy^{3+} phosphor, its CL spectrum (Fig. 2.12b) is made up of the characteristic emission lines of Dy^{3+}, i.e., $^4F_{9/2}$–$^6H_{15/2}$, 491 nm and $^4F_{9/2}$–$^6H_{15/2}$, 580 nm. It has a suitable yellow-to-blue intensity ratio and thus appears a white emission of Dy^{3+} in $SrIn_2O_4$ with CIE chromaticity coordinates $x = 0.3019$ and $y = 0.3291$. The Dy^{3+}-doped $CaIn_2O_4$, $LaGaO_3$ and Ga_2O_3 are also considered as excellent single-phase white-emitting FEDs phosphors with tunable chromaticity coordinates in white light region, as shown in Table 2.2.

2. Codoping different RE^{3+} ions such as Tm^{3+}/Dy^{3+}, Tb^{3+}/Sm^{3+}, Tb^{3+}/Eu^{3+}, Tm^{3+}/Tb^{3+}/Eu^{3+} etc., into single matrix.

Due to the abundant energy levels in 4*f* orbits of RE^{3+} ions such as Tm^{3+}, Dy^{3+}, Tb^{3+}, Sm^{3+}, Eu^{3+} ions, they produce various luminescence colors covering the whole visible light region. Tm^{3+} ion mainly emits blue light around 458 nm due to $^1D_2$–$^3F_4$ transition. Dy^{3+} ion usually exhibits two main emissions in the visible region: one in the blue region (470–500 nm) and one in the yellow region (570–600 nm), which originate from $^4F_{9/2} \rightarrow {}^6H_{13/2}$ and $^4F_{9/2} \rightarrow {}^6H_{15/2}$ transitions of Dy^{3+} ions, respectively. The emission of Eu^{3+} ion mainly appears in red region with the maximum between 610 and 625 nm due to $^5D_0$–$^7F_2$ emission. The emission of Sm^{3+} is situated in the orange spectral region and consists of transitions from the excited $^4G_{5/2}$ level to the ground-state $^6H_{5/2}$ and higher levels ^6H_J ($J > 5/2$). Tb^{3+} ion has a low-energy ground-state ^7F_J ($J = 6, \ldots 0$) and excited states $^5D_3$ and $^5D_4$. Generally, with a low doping concentration of Tb^{3+} in host matrix, the transitions of $^5D_3$ to ^7F_j dominate and produce the blue emissions. As Tb^{3+} concentration

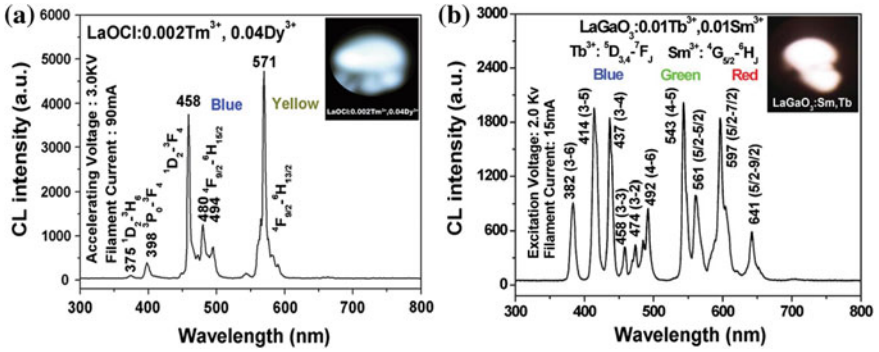

Fig. 2.13 CL spectra and corresponding luminescence photographs of RE^{3+} codoped phosphor systems. **a** LaOCl:Tm^{3+},Dy^{3+} and **b** $LaGaO_3$:Tb^{3+},Sm^{3+}. **a** Adapted from Ref. [41] by permission of Royal Society of Chemistry. **b** Adapted from Ref. [71] by permission of Royal Society of Chemistry

increases, the cross-relaxation from $^5D_3$ to $^5D_4$ occurs owing to the interaction between Tb^{3+} ions, which enhances the transitions of $^5D_4$ to ^7F_j with a green emission. Although these RE^{3+} ions generally are used as single activator in single host, they also generate highly efficient luminescence when coexisting in single matrix. Accordingly, many RE^{3+} ions codoped single-phase phosphor systems were designed to realize white light emission, for example, Tm^{3+}/Dy^{3+}, Tb^{3+}/Sm^{3+}, Tb^{3+}/Eu^{3+}, Tm^{3+}/Tb^{3+}/Eu^{3+} systems, as shown in Table 2.2. Figure 2.13 exhibits the CL spectra and corresponding luminescent photographs of codoping phosphor systems. Under electron beam excitation, LaOCl:Tm^{3+} and LaOCl:Dy^{3+} emit blue light (458 nm, $^1D_2$–$^3F_4$) and yellow light (571 nm, $^4F_{9/2}$–$^6H_{13/2}$), respectively. When codoping Tm^{3+} and Dy^{3+} ions into LaOCl host, it simultaneously gives blue and yellow emission with comparable, which results in a white light emission (CIE coordinates, $x = 0.318$, $y = 0.329$) by the complex of blue and yellow lights (Fig. 2.13a; Table 2.2). For Tb^{3+}/Sm^{3+}-codoped $LaGaO_3$, the white emission is realized by the complex of red, green and blue components. The red component comes from the characteristic transitions of Sm^{3+} (561, 597, 642 nm/$^4G_{5/2}$–$^6H_{5/2}$, $^6H_{7/2}$, $^6H_{9/2}$), while the green and blue components result from the mixing emissions of 414, 437 nm/$^5D_3$–$^7F_{5,4}$; 414, 437 nm/$^5D_4$–$^7F_5$ at a moderate Tb^{3+} doping concentration (Fig. 2.13b; Table 2.2). Based on the same complex method, LaOCl:Tb^{3+}/Eu^{3+}, LaOCl:Tb^{3+}/Sm^{3+}, LaOCl:Tb^{3+}/Eu^{3+}/Tm^{3+} phosphor system also obtained excellent white light emission (Table 2.2). The wide range adjustment of emission colors by precisely controlling the doping contents of RE^{3+} ions makes RE^{3+}-codoped single-phase white light emission have potential application as backlights in FEDs devices.

3. Designing energy transfers from host or RE ions to RE ions or Mn^{2+} ions to in single host.

It is well known that energy transfer plays an important role in the optical properties of luminescent materials both from theoretical and practical points of view, because it can not only enhance the luminescent efficiency but also tune the luminescent color in the single-phase host [92]. The Ce^{3+} with the $4f^1$ configuration in solids shows efficient broad band luminescence due to the $4f-5d$ parity allowed electric dipole transition. It can also act as an efficient sensitizer by transferring a better part of its excitation energy to coactivators. Because the d−d transition of Mn^{2+} is forbidden and difficult to pump, the emission of Mn^{2+} ions is generally excited by energy transfer from the host or the sensitizer. Caldiño [93] reported the spectral overlap between $5d^1 \rightarrow 4f^1$ Ce^{3+} emission and $^6A_1 \rightarrow {}^4T_2$ Mn^{2+} absorption. So far, the $Ce^{3+} \rightarrow Mn^{2+}$ energy transfers have been reported in many inorganic hosts, such as fluorides, phosphates, and borates, and the corresponding mechanisms have been extensively investigated [94, 95]. Ce^{3+} ion can also efficiently transfer energy to Tb^{3+} ions in single host to generate efficient green emission [91]. In these systems, there is a common feature that Ce^{3+} and Mn^{2+}/Tb^{3+} ions simultaneously substitute one or two lattice sites and the Ce^{3+} ions serve as effective sensitizer ions for Mn^{2+}/Tb^{3+}, transferring the energy from the 5D level of the Ce^{3+} to the 4G level of the Mn^{2+} or $^5D_4-{}^7F_j$ level of Tb^{3+} by a process of resonance transfer via a spin exchange mechanism, which not only help Mn^{2+}/Tb^{3+} ions to emit efficiently but also tune their emission colors from blue to yellow or orange/red for $Ce^{3+} \rightarrow Mn^{2+}$, and from blue to green for $Ce^{3+} \rightarrow Tb^{2+}$, across the whole white light region, as shown in Fig. 2.11 and Table 2.2. Some research groups have demonstrated the above situation in many Ce^{3+}–Mn^{2+} (blue-yellow) or Ce^{3+}–Mn^{2+}–Tb^{3+} (blue–red–green) codoped systems such as $Ca_2Ca_8(SiO_4)_6O_2$ [88], $Mg_2Y_8(SiO_4)_6O_2$ [91], $Sr_3In(PO_4)_3$ [96], $Ca_3Sc_2Si_3O_{12}$:Ce^{3+}, Mn^{2+} [97] and so on (Table 2.2). For example, there is an efficient energy transfer from Ce^{3+} to Mn^{2+} in $Ca_2Ca_8(SiO_4)_6O_2$:Ce^{3+}, Mn^{2+}. This phosphor simultaneously emits blue light of Ce^{3+} ions (428 nm) and yellow light of Mn^{2+} ions (490 nm) (Fig. 2.14a), respectively. By changing the relative doping concentration of Ce^{3+} and Mn^{2+}, the ratio of blue to yellow is controllable and thus obtains an excellent white light emission with CIE coordinates (0.342, 0.318). For Ce^{3+}–Mn^{2+}–Tb^{3+}-codoped systems, there simultaneously exist two energy transfer processes of $Ce^{3+} \rightarrow Mn^{2+}$ and $Ce^{3+} \rightarrow Tb^{3+}$, which emit red light and green light, respectively (Fig. 2.14b). Because these energy transfer processes can be controlled via tuning the relative doping concentrations of Ce^{3+}, Tb^{3+} and Mn^{2+} ions. Therefore, the relative emission intensities of blue, green, and red light can be adjusted in single-phase phosphor, resulting in the controllable white light emission (Fig. 2.14b). In summary, by designing efficient energy transfer process $Ce^{3+} \rightarrow Mn^{2+}$ or $Ce^{3+} \rightarrow Mn^{2+}$, Tb^{3+} in single host lattices, excellent white light emission with tunable chromaticity coordinates and high efficiency can be obtained, which is promising in FED backlights. Except for the above energy transfer processes, other energy transfer routes like from Eu^{2+} to Mn^{2+}/Tb^{3+} or from host or self-activated

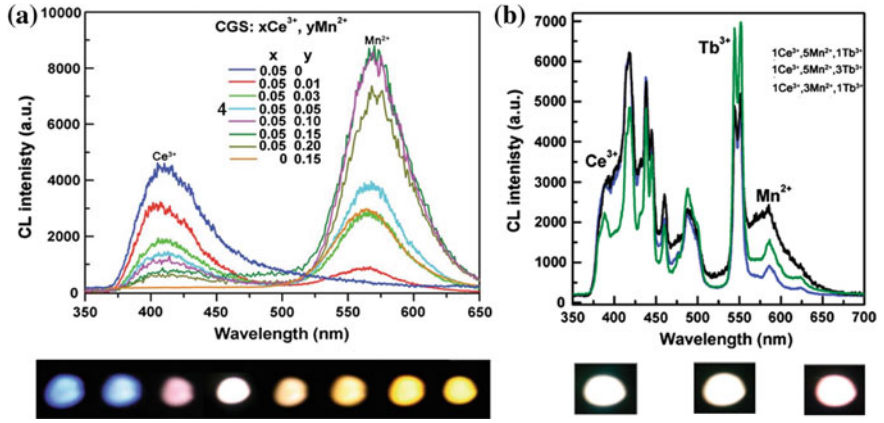

Fig. 2.14 CL spectra and corresponding luminescence photographs of energy transfer phosphor systems: **a** $Ca_2Ca_8(SiO_4)_6O_2:Ce^{3+},Mn^{2+}$ and **b** $Mg_2Y_8(SiO_4)_6O_2:Ce^{3+},Mn^{2+},Tb^{3+}$. **a** Adapted from Ref. [88] by permission of American Chemical Society. **b** Adapted from Ref. [91] by permission of Royal Society of Chemistry

luminescent center to RE^{3+} ions also can gain excellent white light emission, as shown in Table 2.2.

2.3 Development of Novel FEDs Phosphor Powders

Due to a relatively severe operation environment (low-voltage and high current density) in FEDs, future generation phosphors should possess better low-voltage efficiencies, chromaticity (high color purity and wide color gamut), saturation and degradation behavior, and maintenance. Possible routes to achieve these improvements include optimizing morphology, size, surface and crystallization of phosphor grains, enhancing electrical conductivity of phosphors particles, modifying composition of phosphors, enlarging color gamut, designing energy transfers and so on. On the basis of these approaches, in the past decade, a series of novel FEDs phosphors have been developed, as collected in Table 2.3, which shows excellent low-voltage cathodoluminescent properties and has promising application in FED devices. Although most of the newly developed low-voltage FEDs phosphors commonly have the higher color purity and color stability than traditional FEDs phosphors, for examples, LaOCl:Tm^{3+} and $LaGaO_3:Tb^{3+}$ than Y_2SiO_5:Ce (blue) [41]; LaOCl:Tb^{3+} than ZnO:Zn (green) [83]; $(Zn,Mg)_2GeO_4:Mn^{2+}$ and $Mg_2SnO_4:Mn^{2+}$ than $Y_2SiO_5:Tb^{3+}$ (green) [30, 38]; $NaCaPO_4:Mn^{2+}$ than (Zn, CdS):Ag^+ (yellow) [51], their luminescent efficiencies are still lower than the latters. Fortunately, these luminescent disadvantages of the newly developed

Table 2.3 Some newly developed rare earth ions or Mn^{2+} ions activated low-voltage FEDs phosphors and their luminescent properties

Sample	Emission peaks (nm)/main transition	Color	Refs.
$Ga_2O_3:Dy^{3+}$	438/$^4T_1$–$^4A_2$ (GaO_6)	Blue	[32]
	492, 580/$^4F_{9/2}$ to $^6H_{15/2}$, $^6H_{13/2}$ (Dy^{3+})	White	
$CaIn_2O_4:Eu^{3+}$	431, 447, 467, 492, 512, 537, 588, 616/$^5D_{0,1,2,3}$–$^7F_{0,1,2,3}$ (Eu^{3+})	White	[26]
	588/$^5D_1$–$^7F_2$; 619/$^5D_0$–$^7F_2$ (Eu^{3+})	Red	
$SrIn_2O_4:Dy^{3+},Pr^{3+},Tb^{3+}$	493/$^4F_{9/2}$–$^6H_{15/2}$, 582/$^4F_{9/2}$–$^6H_{13/2}$ (Dy^{3+})	Bluish white	[36]
	494/$^3P_0$–$^3H_4$ (Pr^{3+})	Orange	
	487/$^5D_4$–$^7F_6$, 544/$^5D_4$–$^7F_5$ (Tb^{3+})	Green	
$LaOCl:Tm^{3+},Dy^{3+},Sm^{3+},Tb^{3+},Eu^{3+}$	458/$^1D_2$–$^3F_4$ (Tm^{3+})	Blue	[40, 41, 83]
	480, 571/$^4F_{9/2}$ to $^6H_{15/2}$, $^6H_{13/2}$ (Dy^{3+})	Yellow	
	565, 607, 650/$^4G_{5/2}$–$^6H_{5/2,\ 7/2,\ 9/2}$ (Sm^{3+})	Orange	
	384, 416, 437, 486, 543/$^5D_{3,4}$–^7F_j (j = 6-0) (Tb^{3+})	Blue, green	
	615/$^5D_0$–$^7F_2$ (Eu^{3+})	Red	
$LaGaO_3:Tm^{3+},Sm^{3+},Tb^{3+},Dy^{3+},Eu^{3+}$	458/$^1D_2$–$^3F_4$ (Tm^{3+})	Blue	[49, 71]
	561, 597, 642/$^4G_{5/2}$–$^6H_{5/2,\ 7/2,\ 9/2}$ (Sm^{3+})	Yellow	
	414, 437, 414, 437/$^5D_{3,4}$–$^7F_{5,4}$ (Tb^{3+})	Blue, green	
	480, 572/$^4F_{9/2}$ to $^6H_{15/2}$, $^6H_{13/2}$ (Dy^{3+})	Yellowish white	
	590, 614/$^5D_0$–$^7F_{1,\ 2}$ (Eu^{3+})	Red	
$LaInO_3:Eu^{3+}$	465, 491, 512, 534, 588, 610/$^5D_{0,1,2,3}$–$^7F_{0,1,2,3}$ (Eu^{3+})	Yellowish white	[90]
	588, 610/$^5D_0$–$^7F_{1,2}$ (Eu^{3+})	Red	
$Mg_2(Sn,Ti)O_4:Mn^{2+}$	465/(SnO_6)	Blue	[30]
	456/(TiO_6)	Blue	
	499/$^4T_1$–$^6A_1$ (Mn^{2+})	Green	
$Li_2ZnGeO_4:Mn^{2+}$	530/$^4T_1$–$^6A_1$ (Mn^{2+})	Green	[20]
$(Zn,Mg)_2GeO_4:Mn^{2+}$	460/(GeO_6); 531/$^4T_1$–$^6A_1$ (Mn^{2+})	Blue, green	[38]
$NaCaPO_4:Mn^{2+}$	560/$^4T_1$–$^6A_1$ (Mn^{2+})	Yellow	[51]
$Ca_2GeO_4:Eu^{3+}$	613/$^5D_0$–$^7F_2$ (Eu^{3+})	Red	[72]
$CaYAlO_4:Tb^{3+},Eu^{3+}$	383, 416, 468, 537, 548/$^5D_{3,4}$–^7F_j (j = 6-0) (Tb^{3+})	Blue, green	[44]
	593, 623/$^5D_0$–$^7F_{1,2}$ (Eu^{3+})	Red	

low-voltage FEDs phosphors can be reduced or eliminated to some extent through process optimization, including improves the morphology, size and crystallization of phosphors. Therefore, it is very necessary to explore appropriate preparation processes of these phosphors.

2.4 Phosphor Thin Films and Patterning

Except for powders, phosphor thin films that are formed by depositing phosphor precursor on a substrate following a subsequent annealing are the other important form to apply in display faceplates. It appears more attractive for FEDs, because they could be operated at lower voltage and endure much higher power densities without degradation than those powder phosphors [47]. Moreover, phosphor thin films offer advantages such as higher contrast and resolution, better thermal stability, superior thermal conductivity, a high degree of uniformity and better adhesion to the substrate, and reduced outgassing for FEDs compared with the conventional display screen prepared by the direct deposition of phosphor grains [98]. In order to define a smaller pixel spot size, thin film phosphors should possess uniform thickness, smoother surface form and small grain size. To date, phosphor thin films have been prepared by a variety of deposition techniques, such as chemical vapor deposition (CVD), physical vapor deposition (PVD), ion beam sputtering, filtered arc deposition, electrophoretic deposition (EPD), and pulsed laser ablation [99, 100]. These techniques are time-consuming or need expensive and complicated equipment setups. Therefore, a simple and economical method for making high-quality phosphor thin films is desirable, in which the preparation of oxide phosphor films by a PSG process is an excellent candidate [101–103]. This PSG process mainly involve in three steps: the first step is the preparation of a precursor solution with certain viscosity, including the dissolution of the starting materials, formation of metal chelates with citric acid (CA) and their polyesterification with PEG; the second step is the preparation of the amorphous precursor film by a dip-coating or spin-coating process on the desired substrates (silica glasses, silicon wafers, ITO and quartz plates, some ceramics slides, etc.); finally, crystalline phosphor films are produced by the post-annealing process at moderate temperature (500–1000 °C) with a slow heating rate to avoid the cracking and peeling of the films. The as-prepared phosphor thin films via the PSG process have some advantages, as follow: (a) simple process and equipment; (b) low processing temperature, making it possible to prepare films on glass, semiconductor, and integrated photoelectronic devices; (c) films can be coated on substrates with a large area, various shape and different material compositions; (d) a easy control of homogeneity, constituents and microstructure; (e) a controllable thickness by adjusting the viscosity of the coating solution or the repeating number of the coating process. Generally, the phosphor thin films prepared via PSG process are smooth and consist of nanocrystalline grains ranging from 100 to 500 nm. It is noted that the thin film phosphors have lower emission intensity due to the light trapping inside the luminescent layer. Therefore, such films cannot presently compete with powder phosphors in applications phosphors in applications that require high brightness.

On the other hand, full-color displays generally need to deposit the three-color modules (red, green, blue) on the desired regions to form pixels [47]. Therefore, during the fabrication of display devices, patterning luminescent materials on screen

to form pixel matrixes is an essential and critical technique. An accurate patterning technology and screening process for phosphor screen has a vital effect on the resolution of display devices. For instance, pitches of phosphor lines for a super-video graphics adapter with 800 × 600 lines, video graphics adapter with 640 × 480 lines, and quarter video graphics adapter with 320 × 240 lines in 6 in. color displays are defined as 50.8, 63.5, and 127 μm, respectively [47, 104]. So far, electrophoretic deposition, screen printing, vacuum deposition, etc., based on photolithographic patterning technologies have been employed to fabricate FPDs devices [105]. Unfortunately, these patterning techniques for a phosphor screen frequently require expensive photolithographic and etching equipment, complicated layout, and excessive loss of expensive phosphor materials during the fabrication process. Based on these considerations, a growing interest has been focused to soft-lithography patterning techniques, which has the potential of becoming versatile and low-cost methods for creating submicrometer and micrometer size structures [106]. Soft-lithography technique uses a soft and flexible poly (dimethylsiloxane) (PDMS) elastomer that can exactly replicate the surface features of the master mold and transfer them in the patterning process instead of rigid materials as the stamp or mold, and it is carried out by casting the prepolymer on a master with relief structure. Recently, several soft-lithography techniques including micromolding in capillaries (MIMIC), inkjet printing (IP), microtransfer molding (μTM), and microcontact printing (μCP) to realize the pattering of thin film phosphors have been well explored and developed. The detailed introductions are demonstrated in the following sections.

2.4.1 Micromolding in Capillaries (MIMIC)

As soft-lithography technique, MIMIC can pattern a material based on a low-viscosity solution. Phosphor thin films also can be patterned by the MIMIC technique. The basic principle of this process is shown in Fig. 2.15(left). First, polydimethylsiloxane (PDMS) stamp modes (with different channel widths 5–50 μm) were fabricated by casting PDMS on masters having desired patterns [101, 102]. Then the PDMS modes were placed in conformal contact with thoroughly cleaned silicon wafer substrates. The channels of the mode thus formed capillaries with the silicon wafer substrate. The phosphor precursor sol was then dropped at the open end with a transfer pipet. The capillary force made the sol flow into the mold. Then the modes and substrates were dried. After carefully removing the modes, the resulted patterned gel films were heated to high-temperature (500–1000 °C depending on the host compositions) with a slow heating rate (1 °C/min) and held for several hours. In this way, phosphor films with patterning were obtained. Figure 2.15(right) shows optical micrographs of the as-prepared patterned $LaPO_4$: Ce^{3+}, Tb^{3+} gel films. The dark and white regions correspond to the film strips and spaces, respectively. It is clearly seen from a to d in Fig. 2.15(right) that film strips have widths of 5, 10, 20, and 50 μm, respectively, with smooth and perfect

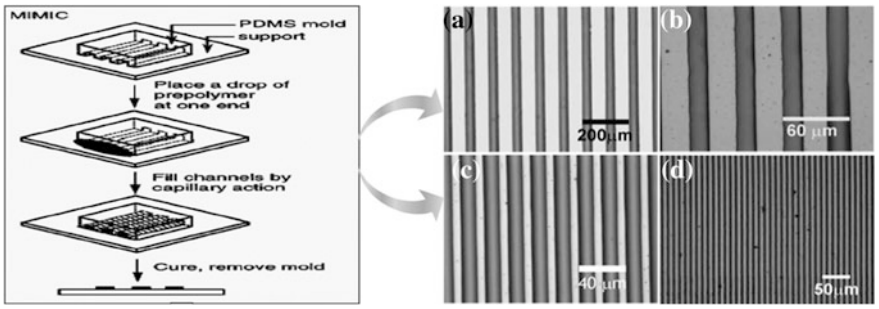

Fig. 2.15 Schematic procedures of MIMIC for patterning of phosphor films (*left*) and the optical photographs for patterned $LaPO_4:Ce^{3+}$, Tb^{3+} phosphor films with different stripe width (*right*, *a* 50 μm, *b* 20 μm, *c* 10 μm, *d* 5 μm). Adapted from Ref. [47] by permission of American Chemical Society

surfaces. Patterned phosphor films were formed after a subsequent annealing of these patterned gel films [101, 102]. According to the MIMIC technique, many other kinds of patterned phosphor films, such as $Y_2O_3:Eu^{3+}$, $Gd_2O_3:Eu^{3+}$, (Y, La, Gd)$VO_4:Eu^{3+}$ etc., can be prepared, which are promising for applications in the FED fields [107, 108].

2.4.2 *Inkjet Printing (IP)*

Recently, inkjet printing has attracted substantial interest as a pathway to make display devices, in which the material deposition and patterning can be performed within a single step by a fully digital driven process [109–111]. This direct-writing technique has many advantages such as simple, fast, large area, and low material consumption. There are many reports for the applications of inkjet printing on the fabrication of polymer light-emitting diodes (PLED) [112, 113]. The deposition of light-emitting polymers as pixels or conducting polymer PEDOT:PSS as the hole transportation layer can be carried out by inkjet printing in the PLED fabrication process. The bottleneck of the inkjet printing technique in organic electronics is being exceeded, and some prototypes of full-color organic light-emitting televisions have been demonstrated. Some attempts have also been made to pattern inorganic phosphor materials for the applications of a field emission flat display by the inkjet printing technique. The inkjet printing system consists of a piezoelectric type printing head with a nozzle (Fig. 2.16a). The microdrops were squeezed out by applying a voltage to the glass capillary inside the dispenser head. A computer-controlled motorized translation stage can move in the X–Y directions relative to the dispenser head which provide the patterns on the substrate such as dots and lines. Using $YVO_4:Eu^{3+}$ as a representative example, the patterning of phosphor thin films through inkjet printing technique can be realized. First, the

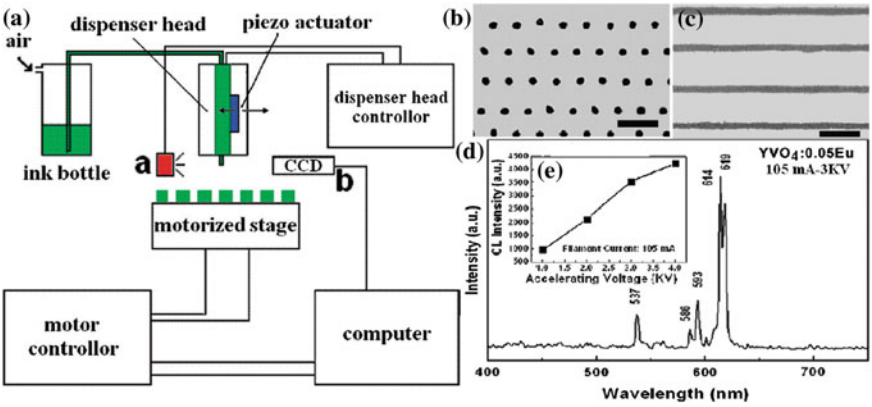

Fig. 2.16 **a** Schematic representation of the inkjet printing setup. **a** The inkjet printing system was manufactured by Microdrop Technique GmbH (Germany), which consists of a piezo-actuated inkjet dispenser head and its controller. A motorized stage under the inkjet printing head equipped with the computer and software provides the precise position of substrate; **b**, **c** microscopy photographs of the as-inkjet-printed *dots* and *lines* of crystalline YVO_4:0.05Eu^{3+}, the *scale bars* represent 200 μm; **d** the CL spectrum of patterned YVO_4:0.05Eu^{3+} on ITO glass excited by electron beam; **e** the CL intensity of the YVO_4:0.05Eu^{3+} pattern as a function of electron beam voltage. Adapted from Ref. [109] by permission of American Chemical Society

YVO_4:Eu^{3+} ink precursor solution was prepared. Then, it was loaded on the inkjet printing system to produce the dots or lines pattern on the ITO glass. After setting driven voltage, pulse width and inkjetting frequency, the YVO_4:Eu^{3+} patterned thin films were obtained. After being dried, the resulting pattern-formed substrates were baked to form the light-emitting YVO_4:Eu^{3+} pixels. Figure 2.16b, c shows the microscopy image of as-inkjet-printed dots array after annealing. Obviously, the as-inkjet-printed dots arrays are highly uniform. Under the excitation of low-voltage electron beam, the patterned YVO_4:0.05Eu^{3+} film can also give red light emission centered at 614 and 619 nm due to the $^5D_0$–$^7F_2$ transition, as shown in Fig. 2.16d. Moreover, the CL intensity increases quickly upon raising the accelerating voltage from 1 to 4 kV when the filament current is fixed on 105 mA, indicating the light-emitting intensity of YVO_4:0.05Eu^{3+} is strongly dependent on the accelerating voltage, which is in line with FEDs working principle. In summary, the preparation of patterning YVO_4:Eu^{3+} light-emitting pixels by a combination of inkjet printing and the PSG method show a feasible scheme for patterning inorganic thin film phosphors by the inkjet printing route (Fig. 2.16e). This facile and quick method has the potential to be used in the fabrication of FEDs devices by continuing efforts to further improving the properties of ink solution and prestructuring substrate, modifying the layout, and so forth.

2.4.3 Microtransfer Molding (μTM)

Microtransfer molding (μTM) is one of the most popular and typical soft-lithography techniques. This technique can directly replicate the feature of the stamp and form the pattern in accordance with the geometry of the stamp. By introducing $YVO_4:Eu^{3+}$ as an example can illustrate the fabrication of light-emitting arrays via μTM technique, as shown in the left of Fig. 2.17a [114]. First, the PDMS stamps were fabricated by casting the PDMS prepolymer, a mixture of Sylgard silicone elastomer and its curing agent over a relief master. The elastomer was degassed and cured and then peeled gently from the master. In this way, PDMS stamps with microwells were obtained. Second, the quartz plates were transformed to hydrophilic properties by immersing them in a piranha solution of concentrated sulfuric acid and hydrogen peroxide. Next, the $YVO_4:Eu^{3+}$ precursor solution was cast on the patterned side of the PDMS mold and the excess solution was removed by scraping with a flat PDMS block. By spin-coating, the $YVO_4:Eu^{3+}$ precursor solution was deposited into the recessed square regions of the PDMS mold, and the mold was brought into contact with the quartz substrate. Then, the mold and substrate were dried. When the mold was peeled away carefully, patterned squares of the $YVO_4:Eu^{3+}$ precursor gels were left on the surface of the quartz substrate. Finally, the patterned substrate was calcined to pyrolyze the organic components and the precursor gel was transformed into crystalline $YVO_4:Eu^{3+}$. The as-prepared $YVO_4:Eu^{3+}$ precursor gel pattern by the μTM technique

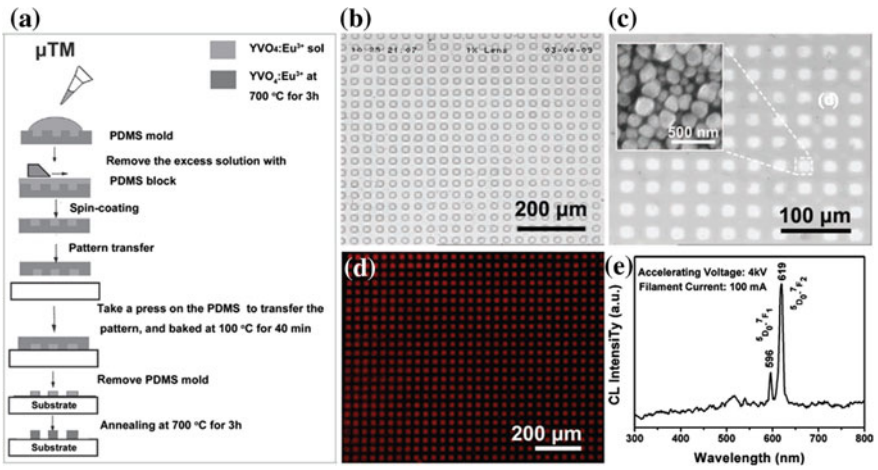

Fig. 2.17 **a** Schematic diagram of the experimental microtransfer molding (μTM) process used for patterning $YVO_4:Eu^{3+}$ films. Optical image of the patterned $YVO_4:Eu^{3+}$ precursor gel film fabricated by **b** μTM, **c** after calcination at 700 °C, and **d** the corresponding luminescent image under 254-nm UV light excitation. The *inset* in **c** SEM image of the patterned $YVO_4:Eu^{3+}$ film, indicative of the morphology of the crystalline $YVO_4:Eu^{3+}$ particles after firing at 700 °C. **e** The CL spectra of the patterned $YVO_4:Eu^{3+}$ film. Adapted from Ref. [114] by permission of Wiley

(Fig. 2.17b) exhibits ordered square arrays without obvious swelling or deformation. After calcination at 700 °C in air, the patterned $YVO_4:Eu^{3+}$ crystalline film was formed on the quartz plate and the corresponding optical microscope image is shown in Fig. 2.17c. A size shrinkage of the square gels was observed after firing, which is attributed to the pyrolysis and evaporation of the organic compounds in the gel. The red luminescent image (Fig. 2.17d) and CL spectrum (Fig. 2.17e) of $YVO_4:Eu^{3+}$ phosphor films indicated that the as-prepared $YVO_4:Eu^{3+}$ phosphor films can be efficiently excited by UV light and low-voltage electron beam.

2.4.4 Microcontact Printing (μCP)

Microtransfer printing (μCP) is another one of the most popular and typical soft-lithography techniques [114]. On the contrast to μTM, the μCP technique prints the self-assembled monolayer (SAM) pattern on the substrate in the first step, which makes the substrate change from being chemically homogeneous into chemically heterogeneous. Then other functional materials can be grown or deposited on the desired patterned regions. Although μCP requires multiple steps and the final pattern formation depends on the chemical heterogeneity of the substrate's surface, these techniques are continuously being developed and improved. For example, a self-assembled monolayer can be firstly transferred onto a substrate and its end group can then be modified through organic synthesis to generate well-defined surfaces with a broad range of characteristics. Therefore, μCP is an improved technique based on μTM. Figure 2.18a shows the process of fabricating a representative $YVO_4:Eu^{3+}$ arrays of dots via μCP. First, the PDMS molds and the quartz plates were carried out the same treatment as μTM technique. The PDMS mold was subsequently flooded with specific organic solvent and blown dry with N_2; then, the PDMS mold was placed in contact with the as-cleaned quartz substrate to print the self-assembled PFOTS monolayer (SAM). Next, the patterned substrate was used as a template for the selective deposition of the metal salts solution by spin-coating. During this spin-coating process, the precursor solution was selectively deposited on the hydrophilic regions because of the poor adhesion between the solution and the SAM. Finally, the substrate with the patterned gel was calcined to obtain the crystalline $YVO_4:Eu^{3+}$ film. The optical microscopy image in Fig. 2.18b shows an ordered dot-patterned $YVO_4:Eu^{3+}$ precursor gel arrays were transferred from the PDMS stamp to the quartz substrate by the μCP technique. After calcination, the patterned $YVO_4:Eu^{3+}$ crystalline film was formed on the quartz plate and the corresponding optical microscope image is shown in Fig. 2.18c. Similarly, the calcination reduces the size of the dot gel spots owing to the pyrolysis and evaporation of the organic species and the edges of the calcined square spots are not as clear as that of the uncalcined gel spots because of the shrinkage during the heat treatment process. Under 254 nm UV light excitation, the patterned $YVO_4:Eu^{3+}$ thin film phosphors show bright red light emission, as shown in Fig. 2.18d. The CL spectra of patterned $YVO_4:Eu^{3+}$ films in Fig. 2.18e also

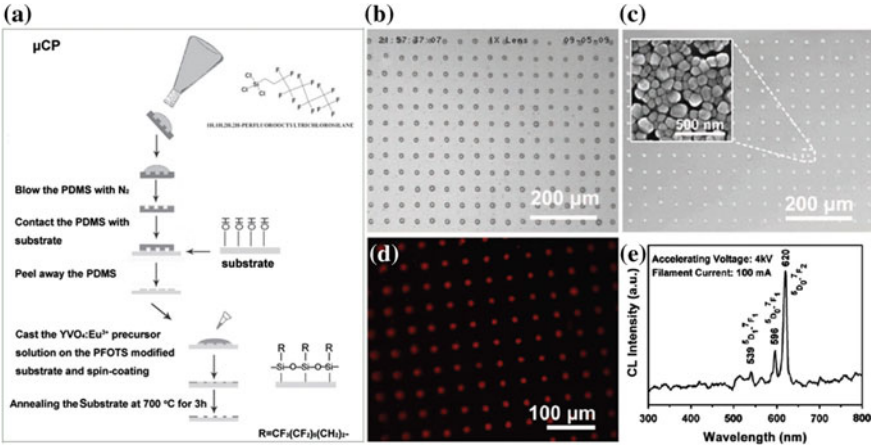

Fig. 2.18 **a** Schematic diagram of the experimental microcontact printing (μCP) process used for patterning $YVO_4:Eu^{3+}$ films. Optical image of the patterned $YVO_4:Eu^{3+}$ precursor gel film fabricated by **b** μCP, **c** after calcination at 700 °C, and **d** the corresponding luminescent image under 254-nm UV light excitation. The *inset* in **c** SEM image of the patterned $YVO_4:Eu^{3+}$ film, indicative of the morphology of the crystalline $YVO_4:Eu^{3+}$ particles after firing at 700 °C. **e** The CL spectra of the patterned $YVO_4:Eu^{3+}$ film. Adapted from Ref. [114] by permission of Wiley

shows the characteristic Eu^{3+} emission at 596 and 619 nm, which correspond to the Eu^{3+} transitions of $^5D_0$–$^7F_1$, and $^5D_0$–F_2, respectively.

Except for $YVO_4:Eu^{3+}$, many other kinds of patterned phosphor films, such as $CaWO_4:Ln^{3+}$ (Ln = Tb, Eu), $Gd_2(WO_4)_3:Ln^{3+}$ (Ln = Eu, Tb) were also prepared based on the μTM and μCP methods, indicating that soft-lithography (μTM and μCP) techniques could be used at all for the patterning of inorganic rare earth salts [115, 116]. These results demonstrate that the Pechini-type sol–gel process has a good compatibility with soft-lithography techniques for patterning inorganic phosphor materials, which holds potential for fabricating new-generation field emission display devices. Moreover, these results can guide us in future research and be helpful to others who have interest in these types of devices.

2.5 Summary and Outlook

Phosphors are irreplaceable components in FEDs devices. The exploring of highly efficient FEDs phosphors has been becoming the focus of realizing high-quality FED. This chapter has summarized the recent progress in chemical synthesis and improvement of FEDs phosphors including rare earth and transition metal ions activated inorganic solid-state luminescent materials, semiconductor-based luminescence materials, self-activated luminescent materials etc. The common strategies for the modifications and optimizations of morphology, size, composition,

conductivity of phosphors, and corresponding effects on their cathodoluminescent properties have also been outlined. Special emphases are mainly focused on the studies of selection of hosts and luminescent centers, enhancement of efficiency through energy transfer, adjustment and design of emission colors, improvement of color index and color gamut as well as color stability and degradation behavior of phosphors. Based on the above modifications and optimizations, the cathodoluminescent performances of phosphors like emission intensity, brightness, color purity, and degradation behaviors can be obviously improved, indicating potential application in full-color FEDs. In addition, single-phase white-light-emitting phosphors with excellent emission properties and tunable CIE chromaticity coordinates have also been developed through designing co-emission and energy transfer between hosts or RE ions and RE ions or Mn^{2+} ions, which are promising backlights in FEDs devices.

Although rapid progress have been achieved in the synthesis, properties, and applications of FEDs phosphors, developing better synthetic routes to further optimize the luminescent performances and more detailed fundamental studies of luminescent mechanisms have a level of urgency. Thus there are still much room for improvement in the future. First, further investigations for optimization the morphology, size, surface state and crystallization of FEDs phosphors need be exactly explored; Secondly, making the matrix maintain a proper electrical conductivity is also a difficult issue; Thirdly, exact degradation mechanism of phosphors under low-voltage electron beam bombardment should be further investigated; Fourthly, researchers with various backgrounds like electronic technology and process optimization may be needed to develop multicolor-system display units and color gamut enlarged phosphors. Finally, numerous efforts need to be made to further develop the single-phase white-emitting luminescence materials based on the energy transfer from sensitizer to activator to contain the advantages of a controllability of emission colors and high luminous efficiency. In addition, the processes and methods for preparing phosphor thin films and screen should be optimized. From a long-term point of view, some emerging phosphors like defect-related environment-friendly phosphors that have high luminous efficiency should be actively explored to open the door to novel display applications. From the point of view of application, the development of highly efficient low-voltage FEDs phosphors might not only promote their application in daily display fields but also offer possibilities for FEDs devices into exploration, expedition, aviation, marine and military fields due to the perfect adaptation of some extremely harsh environment such as very cold or hot conditions. In summary, a large amount of newer improvement methods and novel low-voltage FEDs phosphors are still in the research stage. There is a long way in achieving the high-quality FED and thus need more efforts to pay attention to it.

References

1. Waser, R (2003) Nanoelectronics and Information Technology. chapter 39, Wiley-Vch, Weinheim, Germany
2. Holloway, PH, Trottier, TA, Abrams B, Kondoleon C, Jones SL, Sebastian JS, Thomes WJ, Swart H (1999) Advances in field emission displays phosphors. J Vac Sci Technol B 17: 758–764
3. Höppe, HA (2009) Recent Developments in the Field of Inorganic Phosphors. Angew Chem Int Ed 48: 3572–3582,
4. Jüstel T, Nikol H, Ronda C (1998) New Developments in the Field of Luminescent Materials for Lighting and Displays. Angew Chem Int Ed 37: 3084–3103
5. Hao JH, Gao J, Cocivera M (2003) Green, blue, and yellow cathodoluminescence of $Ba_2B_5O_9Cl$ thin-films doped with Tb^{3+}, Tm^{3+}, and Mn^{2+}. Appl Phys Lett 82: 2224–2226
6. Liu TC, Kominami H, Greer HF, Zhou W, Nakanishi Y, Liu RS (2012) Blue emission by interstitial site occupation of Ce^{3+} in AlN. Chem Mater 24: 3486–3492
7. Zhang QH, Wang J, Yeh CW, Ke WC, Liu RS, Tang JK, Xie MB, Liang HB, Su Q (2010) Structure, composition, morphology, photoluminescence and cathodoluminescence properties of $ZnGeN_2$ and $ZnGeN_2$:Mn^{2+} for field emission displays. Acta Mater 58: 6728–6735
8. Zhang S, Liang HB, Liu CM, Qi ZM, Shao T, Wang YY (2013) High color purity red-emission of $NaGdTiO_4$:Pr^{3+} Via quenching of $^3P_0$ emission under low-voltage cathode ray excitation. Opt Lett 38: 612–614
9. Jing YD, Zhang F, Summers CJ, Wang ZL (1999) Synthesis and properties of Sr_2CeO_4 blue emission powder phosphor for field emission displays. Appl Phys Lett 74: 1677–1679
10. Itoh M, Ozawa L (2006) Cathodoluminescent phosphors. Annu Rep Prog Chem Sect C 102:12–42
11. Han JI, Kwak MG, Park YK, Lim SC, Lee IK, Cho KI, Yoo HJ (1998) Experimental and theoretical considerations on evacuation of vacuum package for field emission display. J Vac Sci Technol B 16: 1236–1238
12. Psuja P, Hreniak D, Strek W (2007) Rare-Earth Doped Nanocrystalline Phosphors for Field Emission Displays. J Nanomater 2007: 81350
13. Wang ZL, Chan HLW, Li HL, Hao JH (2008) Highly efficient low-voltage cathodoluminescence of LaF_3 :Ln^{3+} (Ln = Eu^{3+}, Ce^{3+}, Tb^{3+}) spherical particles. Appl Phys Lett 93: 141106
14. Sharma AK, Son KH, Han BY, Sohn KS (2010) Simultaneous optimization of luminance and color chromaticity of phosphors using a nondominated sorting genetic algorithm. Adv Funct Mater 20: 1750-1755
15. Blasse G, Grabmaier BC (1994) Luminescence Materials (Springer-Verlag, Berlin, Heideberg), ch. 4–5
16. Shi L, Huang YL, Seo HJ (2010) Emission Red Shift and Unusual Band Narrowing of Mn^{2+} in $NaCaPO_4$ Phosphor. J Phys Chem A 114: 6927–6934
17. Liu XM, J. Lin (2007) Enhanced luminescence of gadolinium niobates by Bi^{3+} doping for field emission displays. J Lumin 122–123: 700–703
18. Yamashita T, Ueda K (2007) Blue photoluminescence in Ti-doped alkaline-earth stannates. J Solid State Chem 180: 1410–141319
19. Hou ZY, Li GG, Lian HZ, Lin J (2012) One-dimensional luminescent materials derived from the electrospinning process: preparation, characteristics and application. J Mater Chem 22: 5254–5276
20. Shang MM, Li GG, Yang DM, X. J. Kang, Peng C, Lin J (2012) Luminescence properties of Mn^{2+}-doped Li_2ZnGeO_4 as an efficient green phosphor for field-emission displays with high color purity. Dalton Trans 41: 8861–8868

21. Zhang F L, Yang S, Stoffers C, Penczek J, Yocom PN, Zaremba D, Wagner BK, Summers CJ (1998) Low voltage cathodoluminescence properties of blue emitting $SrGa_2S_4$:Ce^{3+} and ZnS:Ag,Cl phosphors. Appl Phys Lett 72: 2226–2228.
22. Vecht A, Gibbons C, Davies D, Jing X, Marsh P, Reland T, Silver J, Nowport A, Barber D (1999) Engineering phosphors for field emission displays. J Vac Sci Technol B 17: 750–757
23. Guo P, Zhao F, Li G, Liao F, Tian S, Jing X (2003) Novel phosphors of Eu^{3+}, Tb^{3+} or Bi^{3+} activated Gd_2GeO_5. J Lumin 105: 61–67
24. Nagpure IM, Pitale SS, Coetsee E, Ntwaeaborwa OM, Terblans JJ, Swart HC (2011) Low voltage electron induced cathodoluminescence degradation and surface characterization of $Sr_3(PO_4)_2$:Tb phosphor. Appl Surf Sci 257: 10147–10155
25. Srivastava AM, Ronda CR (2003) Phosphors. Electrochem Soc Interface 12: 48–51
26. Liu X, Lin C, Lin J (2007) White light emission from Eu^{3+} in $CaIn_2O_4$ host lattices. Appl Phys Lett 90: 081904
27. Wakefield G, Holland E, Dobson P J, Hutchison JL (2000) Luminescence properties of nanocrystalline Y_2O_3:Eu. Adv Mater 13: 1557–1560
28. Yang SH, Hsueh TJ, Chang SJ (2005) Cathodoluminescence of a white $ZnGa_2O_4$/ZnO phosphor screen. J Electrochem Soc 152: H191–H195
29. Jang HS, Kang JH, Won YH, Lee S, Jeon DY (2007) Mechanism for strong yellow emission of $Y_3Al_5O_{12}$:Ce^{3+} phosphor under electron irradiation for the application to field emission backlight units. Appl Phys Lett 90: 071908
30. Li GG, Zhang X, Peng C, Shang MM, Geng DL, Cheng ZY, Lin J (2011) Cyan-emitting Ti^{4+}- and Mn^{2+}-coactivated Mg_2SnO_4 as a potential phosphor to enlarge the color gamut for field emission display. J Mater Chem 21: 6477–6479
31. Lin CH, Chiou BS, Chang CH, Lin JD (2003) Preparation and cathodoluminescence of ZnO phosphor. Mater Chem Phys 77: 647–654
32. Li GG, Peng C, Li CX, Yang PP, Hou ZY, Fan Y, Lin J (2009) Shape-controllable synthesis and morphology-dependent luminescence properties of GaOOH:Dy^{3+} and β-Ga_2O_3:Dy^{3+}. Inorg Chem 49: 1449–1457
33. Xu XG, Chen J, Deng SZ, Xu NS, Lin J (2010) Cathodoluminescent properties of nanocrystalline $Lu_3Ga_5O_{12}$:Tb^{3+} phosphor for field emission display application. J Vac Sci Technol B 28: 490–494
34. Liu BD, Bando Y, Dierre B, Sekiguchi T, Tang CC, Mitome M, Wu AM, Jiang X, Golberg D (2009) The synthesis, structure and cathodoluminescence of ellipsoid-shaped $ZnGa_2O_4$ nanorods. Nanotechnology 20: 365705–365711
35. Liu XM, Li CX, Quan ZW, Cheng ZY, Lin J (2007) Tunable Luminescence Properties of $CaIn_2O_4$:Eu^{3+} Phosphors. J Phys Chem C 111: 16601–16607
36. Liu XM, Lin CK, Luo Y, Lin J (2007) Host-sensitized luminescence of Dy^{3+}, Pr^{3+}, Tb^{3+} in polycrystalline $SrIn_2O_4$ for field emission displays. J Electrochem Soc 154: J21–J27
37. Jiao H, Wang JG, Liao FH, Tian SJ, Jing XP (2004) Cathodoluminescence of Eu^{3+}, Tb^{3+}, and Tb^{3+}-Eu^{3+} pair-activated $Zn_3Ta_2O_8$. J Electrochem Soc 151: H49–H51
38. Shang MM, Li GG, Yang DM, Kang XJ, Peng C, Cheng ZY, Lin J (2011) (Zn, $Mg)_2GeO_4$:Mn^{2+} submicrorods as promising green phosphors for field emission displays: hydrothermal synthesis and luminescence properties. Dalton Trans 40: 9379–9387
39. Xu XR, Su MZ (2014) Luminescence Science, Luminescent Materials (in Chinese); Chemical Industry Publisher: Beijing
40. Li GG, Hou ZY, Peng C, Wang WX, Cheng ZY, Li CX, Lian HZ, Lin J (2010) Electrospinning derived one-dimensional LaOCl:Ln^{3+} (Ln = Eu/Sm, Tb, Tm) nanofibers, nanotubes and microbelts with multicolor-tunable emission properties. Adv Funct Mater 20: 3446–3456
41. Li GG, Li CX, Zhang CM, Cheng ZY, Quan ZW, Peng C, Lin J (2009) Tm^{3+} and/or Dy^{3+} doped LaOCl nanocrystalline phosphors for field emission displays. J Mater Chem 19: 8936–8943
42. Li GG, Peng C, Zhang CM, Xu, ZH, Shang MM, Yang DM, Kang XJ, Wang WX, Li CX, Cheng ZY, Lin J (2010) Eu^{3+}/Tb^{3+}-doped $La_2O_2CO_3$/La_2O_3 nano/microcrystals with

multiform morphologies: facile synthesis, growth mechanism, and luminescence properties. Inorg Chem 49: 10522–10535
43. Liu XM, Y. Luo, Lin J (2006) Synthesis and characterization of spherical Sr_2CeO_4 phosphors by spray pyrolysis for field emission displays, J Crystal Growth 290: 266–271
44. Geng DL, Li GG, Shang MM, Peng C, Zhang Y, Cheng ZY, Lin J (2012) Nanocrystalline $CaYAlO_4$:Tb^{3+}/Eu^{3+} as promising phosphors for full-color field emission displays. Dalton Trans 41: 3078–3086
45. Zhang Y, Geng DL, Shang MM, X. Zhang, Li XJ, Cheng ZY, Lian HZ, Lin J (2013) Soft-chemical synthesis and tunable luminescence of Tb^{3+}, Tm^{3+}/Dy^{3+}-doped SrY_2O_4 phosphors for field emission displays. Dalton Trans 42: 4799–4808
46. Mao YB, Tran T, Guo X, Huang JY, Shih K Wang KL, Chang JP (2009) Luminescence of nanocrystalline erbium-doped yttria. Adv Funct Mater 19: 748–754
47. Lin J, Yu M, Lin CK, Liu XM (2007) Multiform oxide optical materials via the versatile Pechini-type Sol-Gel process: synthesis and characteristics. J Phys Chem C 111: 5835–5845
48. Liu XM, Zou J P, Lin J (2009) Nanocrystalline $LaAlO_3$:Sm^{3+} as a promising yellow phosphor for field emission displays. J Electrochem Soc 156: P43–P47
49. Liu XM, Lin J (2007) Nanocrystalline $LaGaO_3$:Tm^{3+} as an efficient blue phosphor for field emission displays with high color purity. Appl Phys Lett 90: 184108
50. Liu XM, ZhuL, Wang LL, Yu CC, Lin J (2008) Synthesis and luminescent properties of $Lu_3Ga_5O_{12}$:RE^{3+} (RE = Eu, Tb, and Pr) nanocrystalline phosphors via sol-gel process. J Electrochem Soc 155: P21-P27
51. Li GG, Xu XG, Peng C, Shang MM, Geng DL, Cheng ZY, Chen J, Lin J (2011) Yellow-emitting $NaCaPO_4$:Mn^{2+} phosphor for field emission displays. Opt Exp 19: 16423–16431
52. Geng DL, Shang MM, Zhang Y, Lian HZ, Lin J (2013) Color-tunable and white luminescence properties via energy transfer in single-phase $KNaCa_2(PO_4)_2$:A (A = Ce^{3+}, Eu^{2+}, Tb^{3+}, Mn^{2+}, Sm^{3+}) phosphors. Inorg Chem 52: 13708–13718
53. Geng DL, Shang MM, Yang DM, Zhang Y, Cheng ZY, Lin J (2012) Tunable luminescence and energy transfer properties in $KCaGd(PO_4)_2$:Ln^{3+}/Mn^{2+} (Ln = Tb, Dy, Eu, Tm; Ce, Tb/Dy) phosphors with high quantum efficiencies. J Mater Chem 22: 23789–23798
54. Shang MM, Geng DL, Yang DM, Kang XJ, Zhang Y, Lin J (2013) Luminescence and energy transfer properties of $Ca_2Ba_3(PO_4)_3Cl$ and $Ca_2Ba_3(PO_4)_3Cl$:A (A = Eu^{2+}/Ce^{3+}/Dy^{3+}/Tb^{3+}) under UV and low-voltage electron beam excitation. Inorg Chem 52: 3102–3112
55. Shang MM, Geng DL, Zhang Y, Li GG, Yang DM, Kang XJ, Lin J (2012) Luminescence and energy transfer properties of $Ca_8Gd_2(PO_4)_6O_2$:A (A = Ce^{3+}/Eu^{2+}/Tb^{3+}/Dy^{3+}/Mn^{2+}) phosphors. J Mater Chem 22: 19094–19104
56. Wakefield G, Williams DM, Harris CG, Dobson PJ (2000) Nanocrystalline phosphors for low voltage excitation applications. SID Symposium Digest of Technical Papers 31: 691-693
57. Jung HK, Sohn KS, Sung BY, Park HD (2000) High Luminance Zn_2SiO_4:Mn phosphors prepared by homogeneous precipitation method. J Soc Inf Disp 1: 35-41
58. Silver J, Withnall R, Lipman A, Ireland TG, Fern GR (2007) Low-voltage cathodoluminescent red emitting phosphors for field emission displays. J Lumin 122-123: 562-566
59. Shang MM, Geng DL, Kang XJ, Yang DM, Zhang Y, Lin J (2012) Hydrothermal derived LaOF:Ln^{3+} (Ln = Eu, Tb, Sm, Dy, Tm, and/or Ho) nanocrystals with multicolor-tunable emission properties. Inorg Chem 51: 11106–11116
60. Yang J, Li CX, Cheng ZY, Zhang XM, Quan ZW, Zhang CM, Lin J (2007) Size-tailored synthesis and luminescent properties of one-dimensional Gd_2O_3:Eu^{3+} nanorods and microrods. J Phys Chem C 111: 18148–18154
61. Yang J, Zhang CM, Wang LL, Hou ZY, Huang SS, Lian HZ, Lin J (2008) Self-assembled 3D flowerlike Lu_2O_3 and Lu_2O_3:Ln^{3+} (Ln = Eu, Tb, Dy, Pr, Sm, Er, Ho, Tm) microarchitectures: ethylene glycol-mediated hydrothermal synthesis and luminescent properties. J Phys Chem C 112: 12777-12785

62. Dong GP, Xiao XD, LiuXF, Qian B, Ma ZJ, Chen DP, Qiu JR (2009) Preparation and optical properties of long afterglow europium-doped $Ca(Sr)Al_2Si_2O_8$ electrospun nanofibers. J Electrochem Soc 156: J356–J360
63. Peng C, Hou ZY, Zhang CM, Li GG, Lian HZ, Cheng ZY, Lin J (2010) Synthesis and luminescent properties of $CaTiO_3:Pr^{3+}$ microfibers prepared by electrospinning method. Opt Exp 18: 7543–7553
64. Song HW, Yu LX, Lu SZ (2005) Improved photoluminescent properties in one-dimensional $LaPO_4:Eu^{3+}$ nanowires. Opt Lett 30: 483–485
65. Hou ZY, Yang PP, Li CX,Wang LL, Lian HZ, Quan ZW, Lin J (2008) Preparation and Luminescence Properties of YVO_4:Ln and Y(V, P)O_4:Ln (Ln = Eu^{3+}, Sm^{3+}, Dy^{3+}) Nanofibers and Microbelts by Sol-Gel/Electrospinning Process. Chem Mater 20: 6686–6696
66. Yu M, Lin J, Fang J (2005) Silica spheres coated with $YVO_4:Eu^{3+}$ layers via Sol-Gel process: A simple method to obtain spherical core-shell phosphors. Chem Mater 17: 1783–1791
67. Stöber W, Fink A, Bohn E (1968) Controlled growth of monodisperse silica spheres in the micron size range. J Colloid Interface Sci 26: 62–69
68. Lin CK, Kong DY, Liu XM, Wang H, Yu M, Lin J (2007) Monodisperse and Core-Shell-Structured SiO_2@$YBO_3:Eu^{3+}$ Spherical Particles: Synthesis and Characterization. Inorg Chem 46: 2674–2681
69. Tan SY, Yang PP, Li CX, Wang WX, Wang J, Zhang ML, Jing XY, Lin J (2010) Preparation, characterization and luminescent properties of spherical $CaTiO_3:Pr^{3+}$ phosphors by spray pyrolysis. Solid State Sci 12: 624–629
70. Jung KY, Kim EJ, Kang YC (2004) Morphology control and optimization of luminescent property of YBO_3:Tb phosphor particles prepared by spray pyrolysis. J Electrochem Soc 151: H69-H73
71. Liu XM, Lin J (2008) $LaGaO_3$:A (A = Sm^{3+} and/or Tb^{3+}) as promising phosphors for field emission displays. J Mater Chem 18: 221–228
72. Shang MM, Li GG, Yang DM, Kang XJ, Zhang CM, Lin J (2011) Red emitting $Ca_2GeO_4:Eu^{3+}$ phosphors for field emission displays. J Electrochem Soc 158: J125–J131
73. Yang SH (2004) Indium- and tungsten-doped $ZnGa_2O_4$ phosphor. J Electron Mater 33: L1-L4
74. Kim JY, Jeon DY, Yu I, Yang HG (2000) A study on correlation of low voltage cathodoluminescent properties with electrical conductivity of In_2O_3-coated $ZnGa_2O_4$:Mn phosphors. J Electrochem Soc 147: 3559-3563
75. Xie LP, Song HW, Wang Y, Xu W, Bai X, Dong B (2010) Influence of concentration effect and Au coating on photoluminescence properties of $YVO_4:Eu^{3+}$ nanoparticle colloids. J Phys Chem C 114: 9975-9980
76. Zhang MC, Wang XJ, Ding H, Li HL, Pan LK, Sun Z (2011) The enhanced low-voltage cathodoluminescent properties of spherical $Y_2O_3:Eu^{3+}$ phosphors coated with In_2O_3 and its application to field-emission displays. Int J Appl Ceram Technol 8: 752–758
77. Do YR, Park DH, Yang HG, Park W, Wagner BK, Yasuda K, Summers CJ (2001) Uniform nanoscale SiO_2 encapsulation of ZnS phosphors for improved aging properties under low voltage electron beam excitation. J Electrochem Soc 148: G548-G551
78. Pitale SS, Kumar V, Nagpure IM, Ntwaeaborwa OM, Coetsee E, Swart HC (2011) Cathodoluminescent properties and surface characterization of bluish-white $LiAl_5O_8$:Tb phosphor. J Appl Phys 109: 013105
79. Holloway PH, Swart HC, Ntwaeaborwa OM (2013) Electro-stimulated surface chemical reactions on phosphors. J Vac Sci Technol A 31, 050808.
80. Rag D, Park D, Kim Y (2004) Al_2O_3 Nanoencapsulation of $BaMgAl_{10}O_{17}$: Eu^{2+} phosphors for improved aging properties in plasma display panels. J Electrochem Soc 151: H210-H212
81. Song YH, Xu XC, Zou HF, Sheng Y, You HP (2012) $MSi_2O_{2-\delta}N_{2+2/3\delta}$:Eu (M = Sr, Ba) phosphors for field emission displays. J Alloys Comp 513: 86-90
82. Hetaba W, Mogilatenko A, Neumann W (2010) Electron beam-induced oxygen desorption in γ-$LiAlO_2$. Micron 41: 479-483

83. Li GG, Li CX, Hou ZY, Peng C, Lin J (2009) Nanocrystalline LaOCl: Tb^{3+}/Sm^{3+} as promising phosphors for full-color field-emission displays. Opt Lett 34: 3833–3835
84. Hirosaki N, Xie RJ, Inoue K, Sekiguchi T, Dierre B, Tamura K (2007) Blue-emitting AlN: Eu^{2+} nitride phosphor for field emission displays. Appl Phys Lett 91: 061101
85. Xie MB, Liang HB, Su Q, HuangY , Gao ZH, Tao Y (2011) Intense cyan-emitting of Li_2CaSiO_4:Eu^{2+} under low-voltage cathode ray excitation. Electrochem Solid-State Lett 14: J69-J72
86. Wang DY, Huang CM, Wu YC, Chen TM (2011) $BaZrSi_3O_9$:Eu^{2+}: A cyan-emitting phosphor with high quantum efficiency for white light-emitting diodes. J Mater Chem 21: 10818-10822
87. Bachmann V, Ronda C, Ceckler O, Schnick W, Meijerink A (2009) Color point tuning for (Sr,Ca,Ba)$Si_2O_2N_2$:Eu^{2+} for white light LEDs. Chem Mater 21: 316-325
88. Li GG, Peng C, Li CX, Yang PP, Hou ZY, FanY, Lin J (2011) Tunable luminescence of Ce^{3+}/Mn^{2+}-coactivated $Ca_2Gd_8(SiO_4)_6O_2$ through energy transfer and modulation of excitation: Potential single-phase white/yellow-emitting phosphors. J Mater Chem 21: 13334–13344
89. Huang CM, Wu PJ, Lee JF, Chen TM (2011) (Ca,Mg,Sr)$_9$Y$(PO_4)_7$:Eu^{2+},Mn^{2+}: Phosphors for white-light near-UV LEDs through crystal field tuning and energy transfer. J Mater Chem 21: 10489–10495
90. Liu XM, Yan LS, Lin J (2009) Tunable photoluminescence and cathodoluminescence properties of Eu^{3+}-doped $LaInO_3$ nanocrystalline phosphors. J Electrochem Soc 156: P1–P6
91. Li GG, Geng DL, Shang MM, Zhang Y, Peng C, Cheng ZY, Lin J (2011) Color tuning luminescence of Ce^{3+}/Mn^{2+}/Tb^{3+}-triactivated $Mg_2Y_8(SiO_4)_6O_2$ via energy transfer: Potential single-phase white-light-emitting phosphors. J Phys Chem C 115: 21882–21892
92. Shang MM, Li CX, Lin J (2013) How to produce white light in a single-phase host? Chem Soc Rev 43: 1372-1386
93. Caldiño U (2003) On the Ce-Mn clustering in CaF_2 in which the Ce^{3+}→Mn^{2+} energy transfer occurs. J Phys Condens Matter 15: 3821–3830
94. Zhang CM, Huang SS, Yang DM, Kang XJ, Shang MM, Peng C, Lin J (2010) Tunable luminescence in Ce^{3+}, Mn^{2+}-codoped calcium fluorapatite through combining emissions and modulation of excitation: A novel strategy to white light emission. J Mater Chem 20: 6674–6680
95. Huang CM, Chen TM (2011) A novel single-composition trichromatic white-light $Ca_3Y(GaO)_3(BO_3)_4$:Ce^{3+},Mn^{2+},Tb^{3+} phosphor for UV-light emitting diodes. J Phys Chem C 115: 2349–2355
96. Geng DL, Li GG, Shang MM, Yang DM, Zhang Y, Cheng ZY, Lin J (2012) Color tuning via energy transfer in $Sr_3In(PO_4)_3$:Ce^{3+}/Tb^{3+}/Mn^{2+} phosphors. J Mater Chem 22: 14262–14271
97. Liu YF, Zhang X, Hao ZD, Wang XJ, Zhang JH (2011) Tunable full-color-emitting $Ca_3Sc_2Si_3O_{12}$:Ce^{3+}, Mn^{2+} phosphor via charge compensation and energy transfer. Chem Commun 47: 10677-10679
98. Choe JY, Ravichandran D, Biomquist SM, Morton DC, Kirchner KW, Ervin MH, Lee U (2001) Alkoxy sol-gel derived $Y_{3-x}Al_5O_{12}$:Tb_x thin films as efficient cathodoluminescent phosphors. Appl Phys Lett 78: 3800–3802
99. Li W, Mao DS, Zhang FM, Liu XH, Zou SC, Zhu YK, Li Q, Xu JF (2000) ZnO:Zn phosphor thin films prepared by ion beam sputtering. J Vac Sci Technol A 18: 2295–2301
100. Yum JH, Sung YE (2004) Full color screen by EPD combined with photolithography for flat panel displays. J Electrochem Soc 151: H27–H32.
101. Yu M, Lin J, Wang Z, Fu J, Wang S, Zhang HJ, Han YC (2002) Fabrication, patterning, and optical properties of nanocrystalline YVO_4:A (A = Eu^{3+}, Dy^{3+}, Sm^{3+}, Er^{3+}) phosphor films via Sol-Gel soft lithography. Chem Mater 14: 2224–2231
102. Yu M, Lin J, Fu J, Zhang HJ, Han YC (2003) Sol–gel synthesis and photoluminescent properties of $LaPO_4$:A (A = Eu^{3+}, Ce^{3+}, Tb^{3+}) nanocrystalline thin films. J Mater Chem 13: 1413–1419

103. Pang ML, Shen WY, Lin J (2005) Enhanced photoluminescence of $Ga_2O_3:Dy^{3+}$ phosphor films by Li^+ doping. J Appl Phys 97: 033511
104. Jang JE, Gwak JH, Jin YW, Lee SJ, Park SH, Jung JE, Lee NS, Kim JM (2000) High resolution phosphor screening method for full-color field emission display applications. J Vac Sci Technol B 18: 1106–1110
105. Ying GY, Hu WB, Qiu Y (2002) In The Technology of Flat Panel Displays; Fu, J. Ed.; Post & Telecom Press: Bejing, China
106. Xia Y, Whiteside GM (1998) Soft lithography. Annu Rev Mater Sci 28: 153–184
107. Pang ML, Lin J, Cheng ZY, Fu J, Xing RB, Wang SB (2003) Patterning and luminescent properties of nanocrystalline $Y_2O_3:Eu^{3+}$ phosphor films by sol–gel soft lithograph. Mater Sci Eng B 100: 124–131
108. Pang ML, Lin J, Fu J, Xing RB, Luo CX, Han YC (2003) Preparation, patterning and luminescent properties of nanocrystalline Gd_2O_3:A (A = Eu^{3+}, Dy^{3+}, Sm^{3+}, Er^{3+}) phosphor films via Pechini sol-gel soft lithography. Opt Mater 23: 547–558
109. Cheng ZY, Xing RB, Hou ZY, Huang SS, Lin J (2010) Patterning of light-emitting YVO_4: Eu^{3+} thin films via ink-jet printing. J Phys Chem C 114: 9883–9888
110. Tekin E, Smith PJ, Schubert US (2008) Inkjet printing as a deposition and patterning tool for polymers and inorganic particles. Soft Mater 4: 703–713
111. Singh M, Haverinen HM, Dhagat P, Jabbour GE (2010) Inkjet printing-process and its applications. Adv Mater 22: 673–685
112. Xia YJ, Friend RH (2007) Nonlithographic patterning through inkjet printing via holes. Appl Phys Lett 90: 253513
113. Dijksman JF, Duineveld PC, Hack MJJ, Pierik A, Rensen J, Rubingh JE, Schram I, Vernhout MM (2007) Precision ink jet printing of polymer light emitting displays. J Mater Chem 17: 511–522
114. Wang WX, Cheng ZY, Yang PP, Hou ZY, Li CX, Li GG, Dai YL, Lin J (2011) Patterning of $YVO_4:Eu^{3+}$ luminescent films by soft lithography. Adv Funct Mater 21: 456–463
115. Wang WX, Yang PP, Cheng ZY, Hou ZY, Li CX, Lin J (2011) Patterning of red, green, and blue luminescent films based on $CaWO_4:Eu^{3+}$, $CaWO_4:Tb^{3+}$, and $CaWO_4$ phosphors via microcontact printing route. ACS Appl Mater & Interfaces 3: 3921–3928
116. Wang D, Yang PP, Cheng ZY, Wang WX, Hou ZY, Dai YL, Li CX, Lin J (2012) Patterning of $Gd_2(WO_4)_3:Ln^{3+}$ (Ln = Eu, Tb) luminescent films by microcontact printing route. J Coll Inter Sci 365: 320–325

http://www.springer.com/978-981-10-1589-2

Phosphors, Up Conversion Nano Particles, Quantum Dots and Their Applications
Volume 2
Liu, R.-S. (Ed.)
2016, VIII, 523 p. 303 illus., 263 illus. in color.,
Hardcover
ISBN: 978-981-10-1589-2